A TRIDENT SCHOLAR PROJECT REPORT

NO. 162

Viscous Drag Reduction
for
Slender Surface Craft

UNITED STATES NAVAL ACADEMY
ANNAPOLIS, MARYLAND

UNCLASSIFIED

SECURITY CLASSIFICATION OF THIS PAGE *(When Data Entered)*

REPORT DOCUMENTATION PAGE		READ INSTRUCTIONS BEFORE COMPLETING FORM
1. REPORT NUMBER U.S.N.A. - TSPR; no. 162 (1989)	2. GOVT ACCESSION NO.	3. RECIPIENT'S CATALOG NUMBER
4. TITLE *(and Subtitle)* VISCOUS DRAG REDUCTION FOR SLENDER SURFACE CRAFT.		5. TYPE OF REPORT & PERIOD COVERED Final 1988/89
		6. PERFORMING ORG. REPORT NUMBER
7. AUTHOR*(s)* David B. Walker		8. CONTRACT OR GRANT NUMBER*(s)*
9. PERFORMING ORGANIZATION NAME AND ADDRESS United States Naval Academy, Annapolis.		10. PROGRAM ELEMENT, PROJECT, TASK AREA & WORK UNIT NUMBERS
11. CONTROLLING OFFICE NAME AND ADDRESS United States Naval Academy, Annapolis.		12. REPORT DATE 7 July 1989
		13. NUMBER OF PAGES
14. MONITORING AGENCY NAME & ADDRESS*(if different from Controlling Office)*		15. SECURITY CLASS. *(of this report)*
		15a. DECLASSIFICATION/DOWNGRADING SCHEDULE

16. DISTRIBUTION STATEMENT *(of this Report)*

This document has been approved for public release; its distribution is UNLIMITED.

17. DISTRIBUTION STATEMENT *(of the abstract entered in Block 20, if different from Report)*

18. SUPPLEMENTARY NOTES

Accepted by the U.S. Trident Scholar Committee.

19. KEY WORDS *(Continue on reverse side if necessary and identify by block number)*

Ship resistance
Viscous flow
Frictional resistance (Hydrodynamics)

20. ABSTRACT *(Continue on reverse side if necessary and identify by block number)*

The object of this research was to investigate viscous drag reduction methods that may be applied to certain marine vehicles. These methods include the injection of microbubbles into the boundary-layer and the use of riblets and various transition-control devices. Experiments were performed in the USNA towing tank with two single rowing shells (hull shapes for which the viscous resistance is the dominant component of

(OVER)

resistance). Resistance, sinkage, and trim were measured for speeds up to 20 ft/sec. In the case of air injection, the residual resistance was a function of interactive viscous, form, and wave making components making it difficult to ascertain whether or not the viscous component was actually reduced, despite the increase in overall resistance. Riblet surfaces produced up to 3 to 4 percent o erall vehicle drag reduction, which is consistent with previous results for rowing shells and predicted values for a form whose frictional resistance accounts for about 85 percent of the total resistance. While the overall vehicle drag was increased with the addition of a trip wire to the bare hull at low velocities, there was drag reduction up to 2 to 3 percent at the highest velocities, possibly due to venting of the trip wire. The maximum drag reduction of about 6 percent was obtained with both riblets and trip wire for the maximum velocity of 20 ft/sec. Results for the combination of riblets and trip wire were apparently additive across the velocity range of the experiment.

Viscous Drag Reduction

for

Slender Surface Craft

A Trident Scholar Project Report

by

Midshipman David B. Walker

U.S. Naval Academy

Annapolis, Maryland

David W. Coder

Research Advisor: Dr. David W. Coder

Roger H. Compton

Faculty Advisor: Professor Roger H. Compton
Naval Systems Engineering

Vernon C. Gaudin for M. Saarlas

Department Advisor: Professor Michael Saarlas
Aerospace Engineering

Accepted for Trident Scholar Committee

Dennis F. Hasson

Chairperson

7 July 1989

Date

USNA 1531-2

ABSTRACT

The objective of this research was to investigate viscous drag reduction methods that may be applied to certain marine vehicles. These methods include the injection of microbubbles into the boundary-layer and the use of riblets and various transition-control devices. Experiments were performed in the USNA towing tank with two single rowing shells (hull shapes for which the viscous resistance is the dominant component of resistance). Resistance, sinkage, and trim were measured for speeds up to 20 ft/sec. In the case of air injection, the residual resistance was a function of interactive viscous, form, and wave making components making it difficult to ascertain whether or not the viscous component was actually reduced, despite the increase in overall resistance. Riblet surfaces produced up to 3 to 4 percent overall vehicle drag reduction, which is consistent with previous results for rowing shells and predicted values for a form whose frictional resistance accounts for about 85 percent of the total resistance. While the overall vehicle drag was increased with the addition of a trip wire to the bare hull at low velocities, there was a drag reduction up to 2 to 3 percent at the highest velocities, possibly due to venting of the trip wire. The maximum drag reduction of about 6 percent was obtained with both riblets and trip wire for the maximum velocity of 20 ft/sec. Results for the combination of riblets and trip wire were apparently additive across the velocity range of the experiment.

TABLE OF CONTENTS

LIST OF TABLES

LIST OF FIGURES

LIST OF SYMBOLS

C_D	Parasite drag coefficient of trip wire
$(C_F)_{ITTC}$	ITTC friction resistance coefficient
C_{FORM}	Form drag coefficient
C_R	Residual resistance coefficient
C_{R0}	Residual resistance coefficient (bare hull)
C_{R0}^*	Residual resistance coefficient (bare hull & trip)
C_T	Total resistance coefficient
C_{T0}	Total resistance coefficient for bare hull
C_{T0}^*	Total resistance coefficient for bare hull with trip wire
$(C_T)_Q$	Total resistance coefficient for non-zero air flow
$(C_T)_{Q=0}$	Total resistance coefficient for zero air flow
D	Diameter of trip wire
F_n	Froude number
g_{tw}	Wetted girth of trip wire
h	Height of riblets
h^+	Non-dimensional height
k	Roughness height
l	Length of shell
Q_a	Air flow rate
Q_w	Water flow rate
r	Hughes form factor

R	Total resistance
R_k	Reynolds number based on roughness height
R_l	Reynolds number based on length to trip wire
R_n	Reynolds number
s	Spacing of riblets
s^+	Non-dimensional spacing
S	Wetted surface area of shell at $F_n = 0$
U_k	Velocity at top of roughness
v^*	Shear velocity
W_e	Weber number
$(\Delta C_F)_{RIB}$	Change in C_F due to addition of riblets
$(\Delta C_R)_{RIB}$	Change in C_R due to addition of riblets
$(\Delta C_T)_{AJ}$	Change in C_T due to addition of air jacket
$(\Delta C_T)_{BLOW}$	Change in C_T due to air injection
$(\Delta C_T)_{RIB+TRIP}$	Change in C_T due to addition of riblets and trip
$(\Delta C_T)_{TRIP}$	Change in C_T due to addition of trip wire
ν	Kinematic viscosity
σ	Surface tension

INTRODUCTION

Fluid mechanical drag adversely affects the performance of all vehicles that travel through a fluid medium. It limits the maximum speed for a given installed power and limits range or endurance for a given amount of stored energy. With the ability to reduce drag comes the possibility to extend the speed and range or reduce the power requirements of these vehicles. Efforts to reduce drag have included streamlining/fairing and inducing turbulent flow with roughness to reduce flow separation and pressure drag at low Reynolds numbers. Delaying transition from laminar to turbulent flow has also been investigated to increase the portion of laminar flow with its inherently lower value of skin friction. To mitigate the increased momentum transfer that is characteristic of turbulent flow, methods and/or devices such as surface smoothing, compliant coatings, polymer injection, large eddy break-up devices, air injection, and riblet surfaces have been studied for control of turbulence or the factors leading to turbulence. The present project focuses on the use of riblets and air injection as potential drag reduction devices for marine vehicles as well as the effect on the total vehicle drag of adding various tripping devices.

Riblets, or small longitudinal grooves in the surface

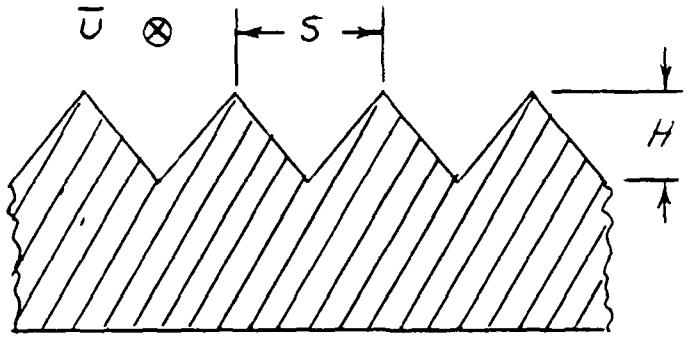

$$S = H = 0.003 \text{ in.}$$

$$S^+ = S v^* / \nu$$

$$v^* = (\tau_w / \rho)^{1/2} = U (C_f/2)^{1/2}$$

Figure 1 Riblets in cross section

[Figure 1], have been shown by Walsh and Lindemann [1984] at the National Aeronautics and Space Administration (NASA) and Reidy and Anderson [1988] at the Naval Ocean Systems Center (NOSC) to produce as much as 8 percent turbulent flow drag

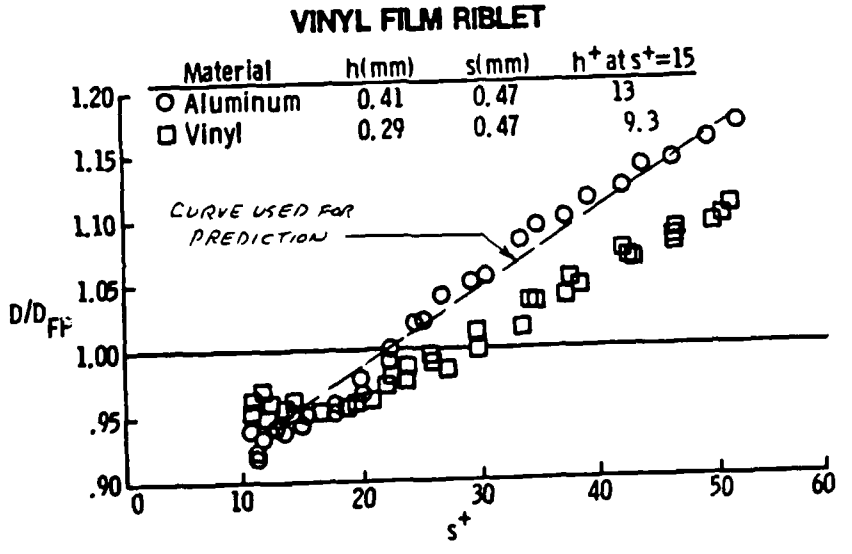

Figure 2 Drag Reduction on a flat plate with riblets (NASA)

reduction on flat plates for an s^+ of 12-13 with $h \approx s$ [Figure 2] and are projected to be optimized at perhaps 10 percent. Skin friction reductions of 7 percent were achieved with riblets on fully submerged axisymmetric bodies in water at the Naval Underwater Systems Center (NUSC) by Beauchamp and Philips [1986 and 1987]. Several series of tests have been conducted using riblets on single racing shells by Coder at the David Taylor Research Center (DTRC) (see Eilers et al. [1984]) for the U.S. Olympic Rowing team and McKelvey [1988] in the 380 ft towing tank at the U.S. Naval Academy (USNA) which led to overall drag reductions of 3 to 3.5 percent. Based on the projected optimized results, one might expect a marine vehicle with 80 percent of total drag due to turbulent flow skin friction (typical of a submarine or torpedo) to attain a potential drag reduction of 8 percent (10 percent x 80 percent). Assuming that power is approximately proportional to velocity cubed, an overall vehicle drag reduction of 8 percent would mean a 2 percent increase in velocity or range for the same installed power or an 8 percent reduction in required power or an 8.7 percent increase in range for the same velocity. These potential benefits along with the commercial development of riblet tape (that allows simple application of riblets to almost any surface) were the driving factors and the means for initiating the present project.

Microbubbles have the potential, in certain applications, to yield significantly greater drag reduction than riblets, with commensurate increase in vehicle performance. The difficulty of maintaining a stable layer of air prevented any effective experimental investigation of this potential until the last 20 years. McCormick and Bhattacharya [1973] used electrolysis on fine wires wrapped around an axisymmetric body to produce a layer of air. Total vehicle drag reductions of 30-40 percent were reported, decreasing to a total drag reduction of 10 percent at the highest velocities. Further tests of the electrolysis method, using larger models, were reported by Thornton [1974] and McCormick [1989]. The test speed was limited to 5 ft/s, where only 2.3 percent drag reduction was measured. The experiment used a limited current supply, so it is difficult to say whether more drag reduction could have been achieved or what results might be obtained at higher speeds.

There have since been several Soviet studies conducted by Migirenko et al. [1974], Dubnishev et al. [1975], and Bogdevich and Malyuga [1976] using small bubbles created by forcing air through porous media. Local skin friction reductions of as much as 90 percent were reported for a wide range of flow conditions and for injection surfaces with various porosities. In general, the amount of turbulent skin friction decreased with increasing flow rate until some

maximum saturation value. These results have been corroborated and extended by several researchers at the Applied Research Laboratory/Pennsylvania State University (ARL/PSU). Madavan et al. [1984] reported on an experiment in a zero-pressure-gradient, turbulent boundary layer on a floating element drag balance mounted in the wall of a water tunnel. Microbubbles were generated on an upstream porous plate which could be mounted on the top, bottom, or side of the tunnel in order to study buoyancy effects. Porous stainless steel having a nominal filter rating of 0.5 microns was used. Deutsch and Castano [1986] used an axisymmetric body with a parallel section floating free of the nose and base sting on a force-measuring gauge. A nominal pore size of 5 microns was used, and the streamwise length of the injector section was much less than that of the flat plate used by Madavan. The significant results of these studies are shown in Figures 3 and 4 and included a maximum skin friction reduction of 80 percent at high flow rates, microbubble effectiveness persisting 60 to 70 boundary layer thicknesses downstream of the injection point at high flow rates, drag reduction dependence on a high unit Reynolds number, and an optimum volumetric fraction of air in the boundary layer ($Q_a/(Q_a+Q_w)$) of approximately 0.3. Any power savings achieved through this form of "active" drag reduction must, of course, compensate for the power that must be diverted to generate the

microbubbles. These forced air experiments were all performed on simple shapes. It appears that no marine vehicle applications have been reported. In the present study, the emphasis was placed on the surface vessel application, with its unlimited supply of air and relatively low hull pressures.

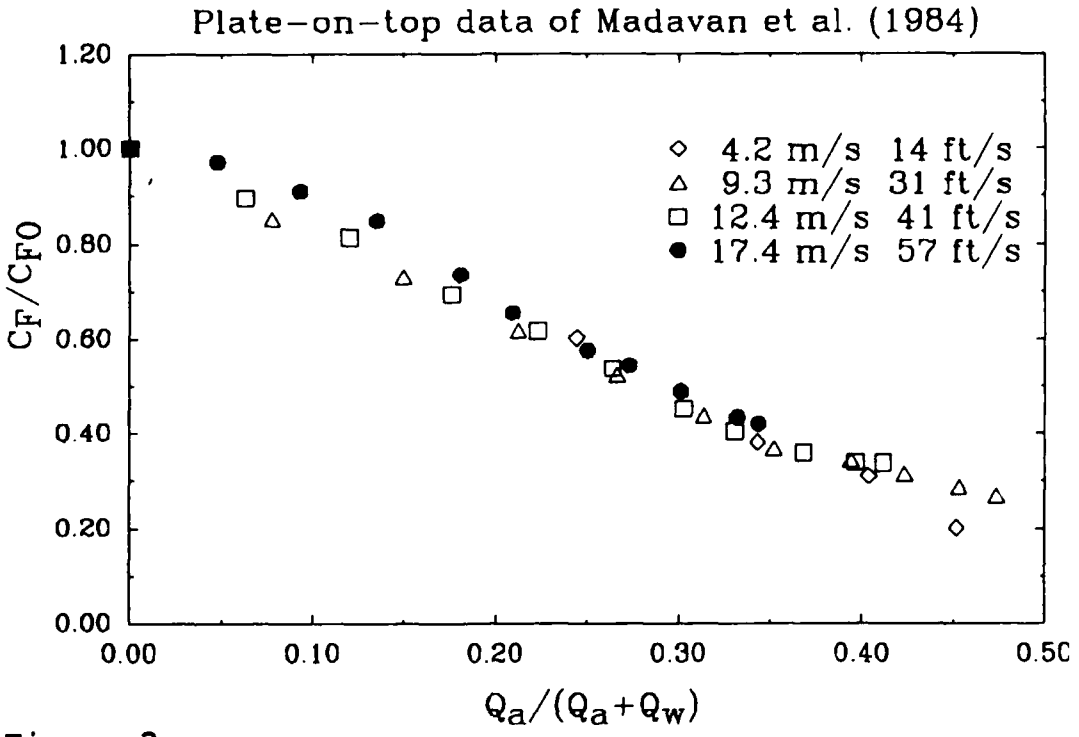

Figure 3

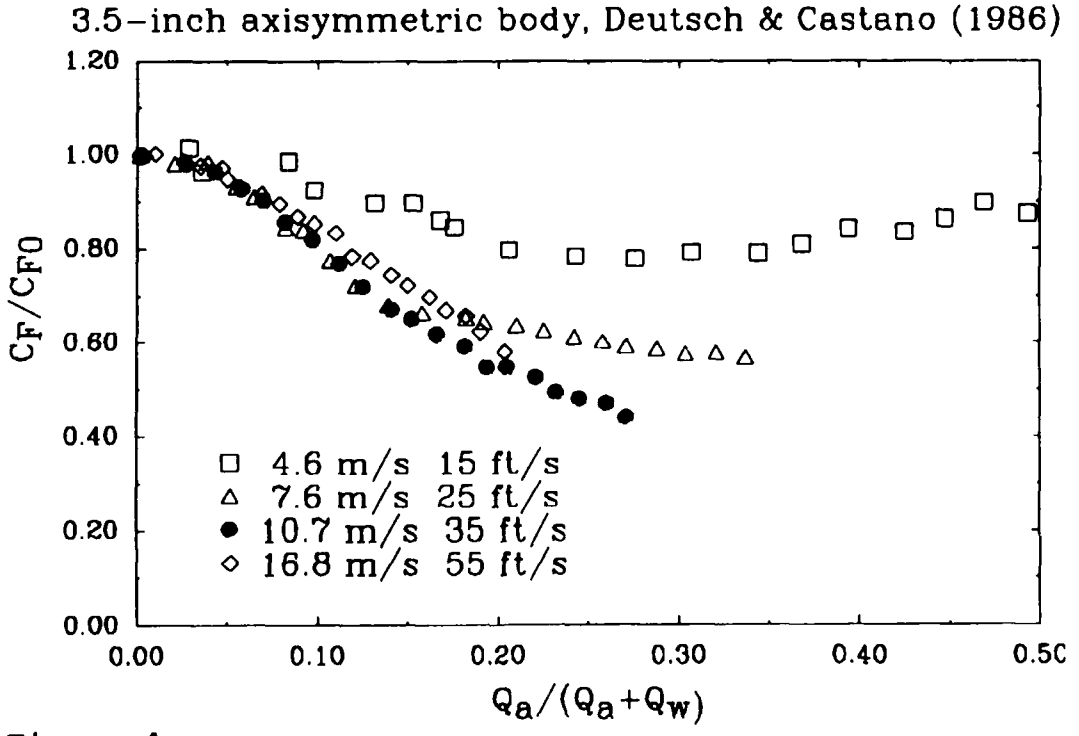

Figure 4

EXPERIMENTAL PROGRAM

RIBLET EXPERIMENTS

In order to verify the drag reduction properties of riblet tape on marine vehicles, two single rowing shells, one white and one yellow, were borrowed from the USNA rowing team to provide hull shapes for which the viscous resistance is the dominant component (about 85 percent). The shells were outfitted as shown in Figure 5. The outriggers were removed and ballast added for stability and to obtain the same waterline as would be obtained with a 200 lbf oarsman aboard. For each shell, this waterline was marked and the wetted girth measured along its length. From these and measurements of the overall length, the midship section shape, and the displacement, a set of approximate lines was developed using the FASTSHIP computer program. Plots of these lines are given in the Appendix along with the naval architectural characteristics of the hulls. As seen in Figure 6, the shells have a 1/8 in.-wide, 5/8 in.-high skeg around the outside of the hull on the hull centerplane. The shell is molded in halves and joined on the centerline by means of this skeg. This was used in the experiments conducted by McKelvey [1988] to run an air tube down the stem of the model to the area that was to accommodate the riblet surface. An 1/8 in. copper tube

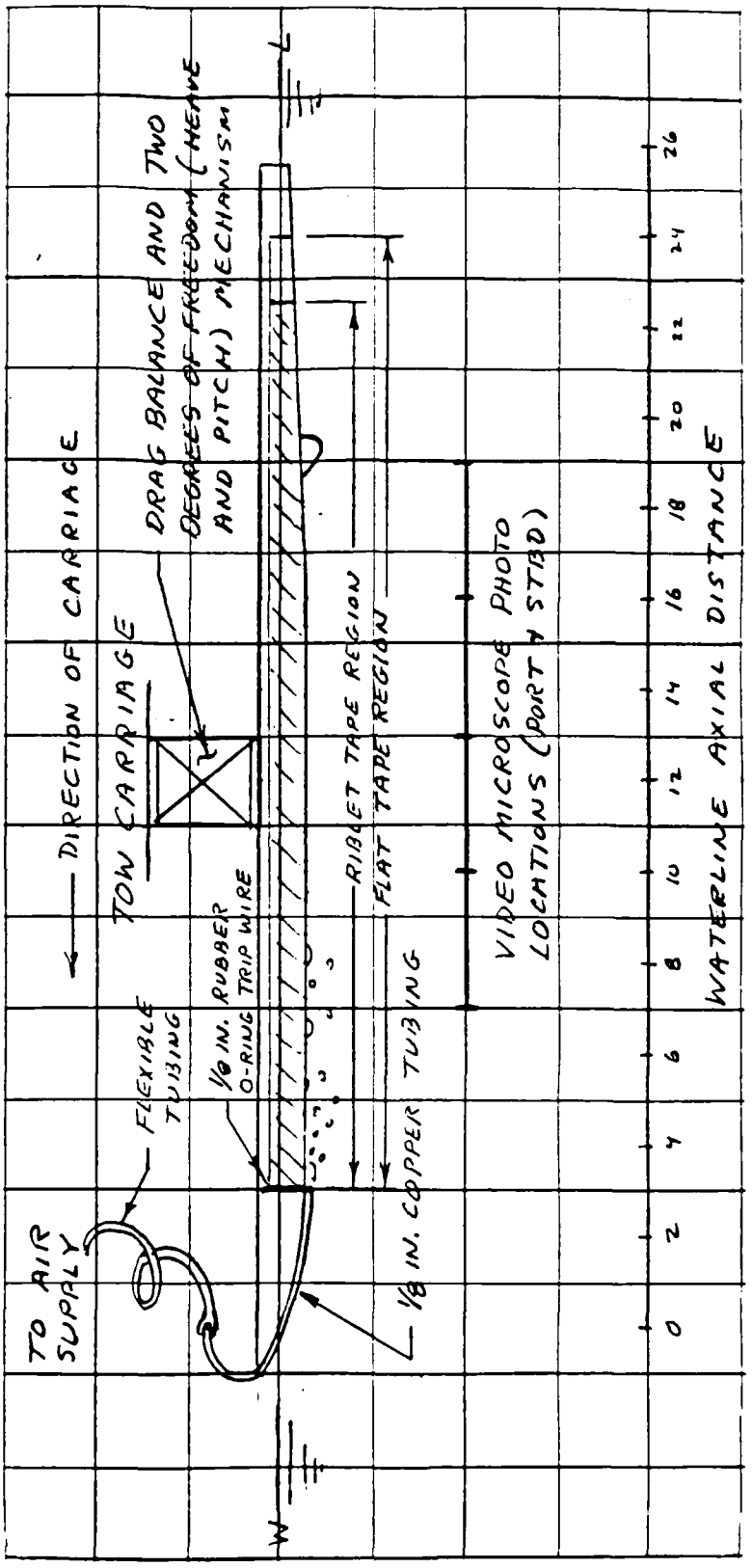

Figure 5 Schematic of shell and experimental arrangement

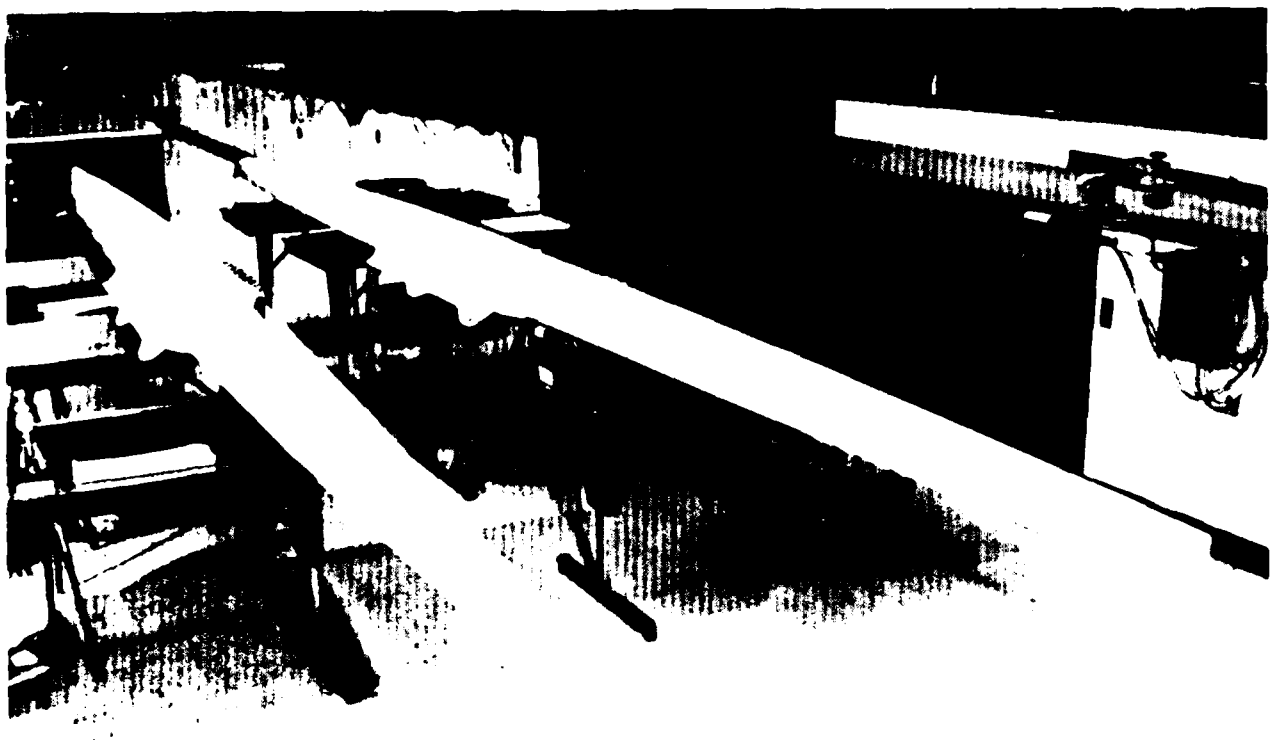

Figure 6 White and yellow shells in lab

was bent around the stem and attached to this skeg so that the upper end could be attached to a flexible hose leading to an air supply and the lower end would deliver air 3 ft aft of the forward perpendicular on the centerline-bottom of the shell [Figure 7]. In this manner, the tube was placed out of the hull boundary layer and was expected to have minimal effect on the hull boundary layer development and transition. The longitudinal location for the leading edge of the riblet and/or flat tape (used by McKelvey [1988] for baseline measurements) surface was chosen to be aft of the predicted natural transition location for most of the higher velocities that were to be tested. It was expected that transition might occur on the riblet surface for some of the lower velocities. It was hoped that this phenomenon (a drag change due to the extension of laminar flow with riblets) could be examined as well as turbulent flow drag reduction. The procedure to install the riblet tape is shown in Figure 8.

For some of the testing, trip wires were added to the hull in an attempt to fix the transition location. Small trip wires of 1/16-in. diameter and large ones of 1/8-in. diameter were fastened to the hull around the girth from above the waterline to the middle of the radius between the hull and the skeg. The longitudinal location of the trip was either 2 ft

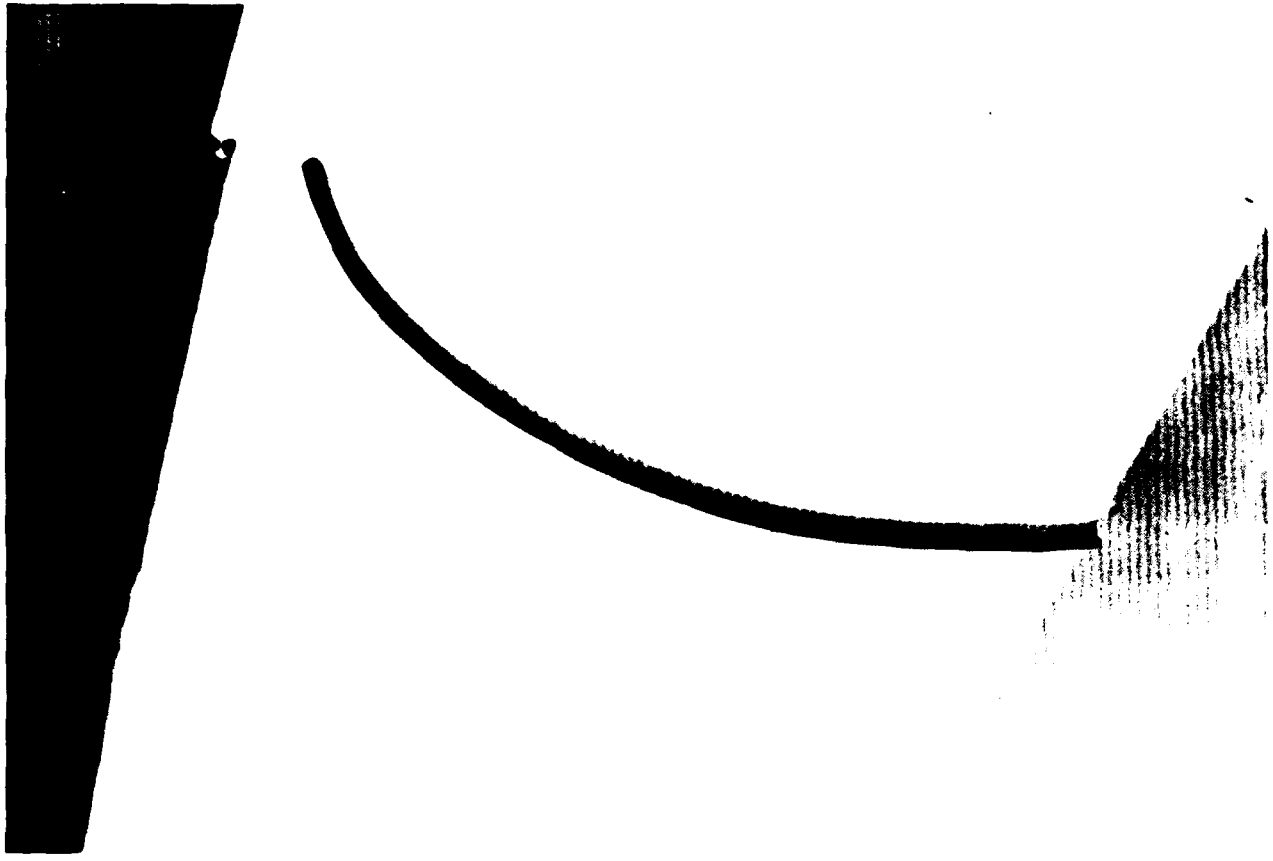

Figure 7 White shell showing showing air tubing

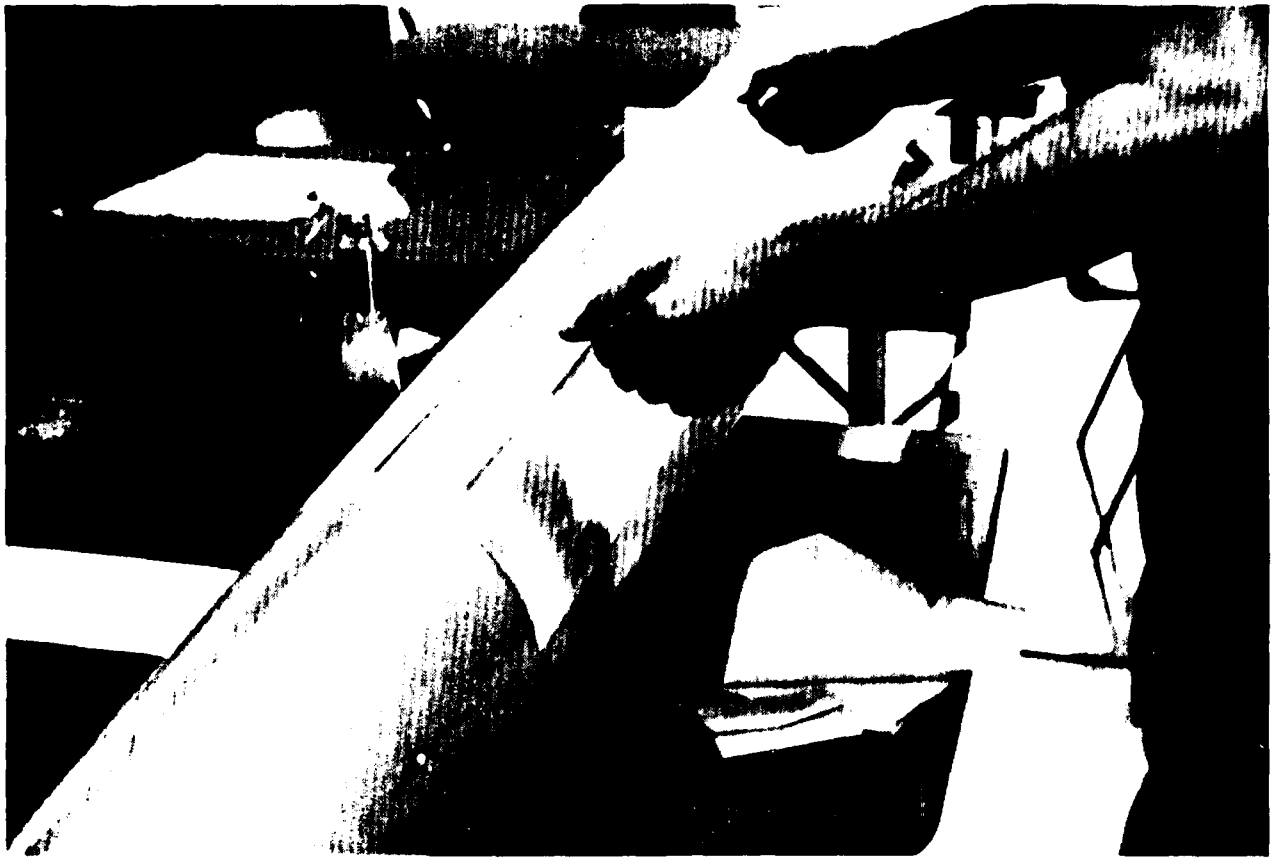

Figure 8 Application of riblet tape

(forward position), 3 ft (middle position), or 4 ft (aft position) aft of the zero velocity waterline entry. Figure 9 shows the large trip wire attached to the white shell at the middle position.

From McCarthy et al. [1976], it is presumed that the boundary layer will transition from laminar to turbulent flow as long as

$$R_l > 10^4, \text{ and}$$

$$R_k = U_k k/\nu > 600$$

From flat plate boundary layer calculations, it was determined that a trip wire of 1/8 in. diameter at the middle location would meet the above criteria for most of the test velocities. In order to obtain a data-base of information for tripping with and without riblets, the smaller trip wire was also selected for testing, along with several longitudinal locations on the shell. However, due to the complexity of including sinkage, trim, vibration and turbulence-in-the-tank effects, the determination of the optimum riblet-tripping combination is beyond the scope of the present work.

The shells were attached to the mounting plate of the resistance dynamometer on the carriage in the USNA 380 ft tow tank (see ITTC [1971,1977,1980]) by clamping the plate

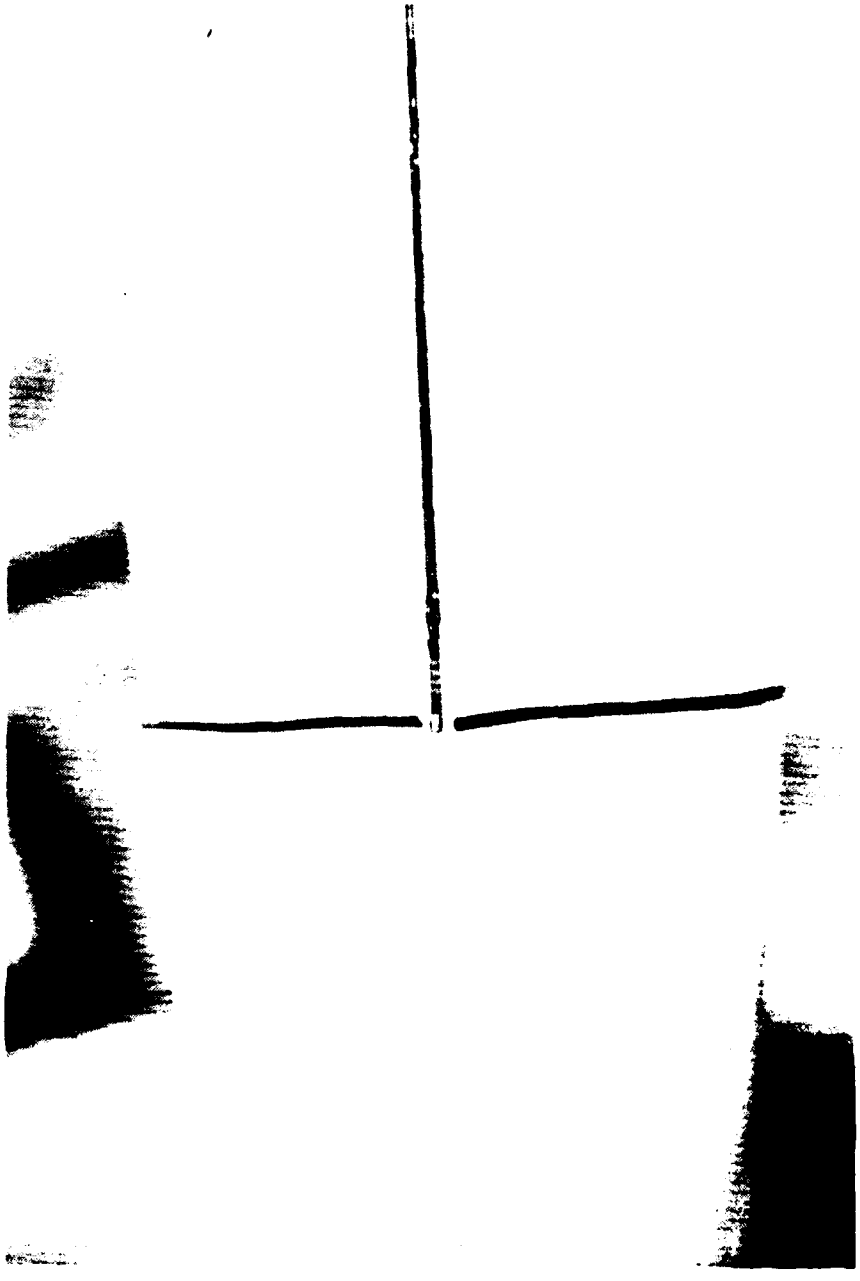

Figure 9 White with large trip wire at middle location

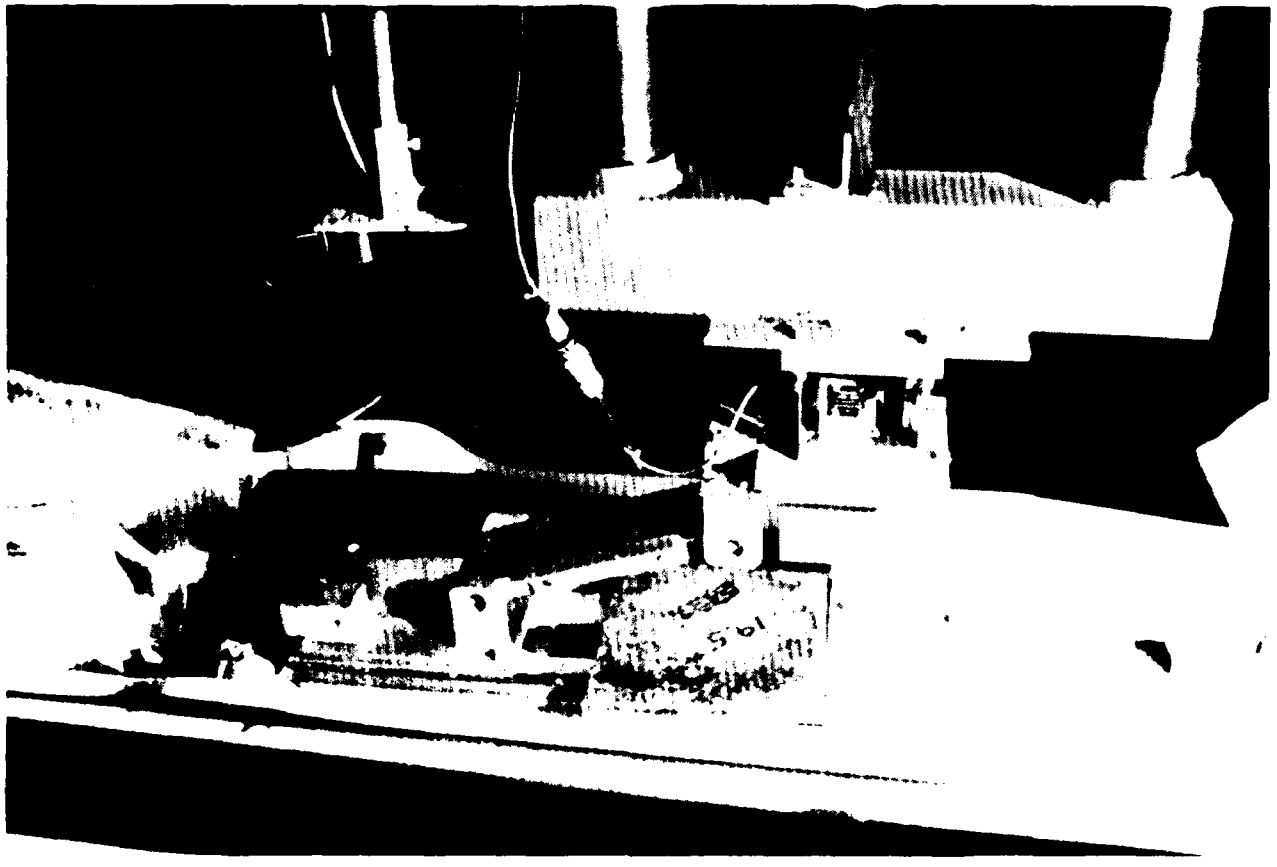

Figure 10 Cockpit area showing attachment mechanism

to the shell seat track [Figure 10]. The attachment mechanism allowed the shell to move freely in sinkage and trim while restraining it in yaw, sway, roll, and surge. The resistance was measured with a variable reluctance force block, sinkage with a sonic height probe, and trim with an inclinometer [Figure 10].

Experiments in the USNA tow tank were conducted over a three-month period from December 1988 to February 1989. Data were obtained over a range of speeds from 4 to 20 ft/sec in 2 ft/sec increments. The test matrix is given in Table 1 which includes the tests conducted by McKelvey from March to June 1988.

Table 1: Test matrix

SHEET	DATE (MDY)	SHELL (W/Y/YM)	COATING (B/F/R)	TRIP WIRE (0/S/L)	TRIP LOC (F/M/A)	AIR FLOW (CFM)
1	030188	W	B			
2	030488	W	F			
3	030488	Y	F			
4	030988	Y	R(1ST)			
5	031088	W	R(1ST)			
6	031088	Y	R(2ND)			
7	031188	Y	R(3RD)			
8	031188	W	R(2ND)			
9	031488	W	R(3RD)			
10	042288	W	R	L	M	
11	042288	Y	R	L	M	
12	060288	Y	B	L	M	
13	060288	W	B	L	M	
14	121488	W	B	0		
15	121588	W	B	L	A	
16	121688	W	B	L	F	
17	121688	W	B	L	M	
18	122088	YM	B	L	M	0
19	122088	YM	B	L	M	10
20	122088	YM	B	L	M	20
21	122188	YM	B	L	M	30
22	122188	YM	B	L	M	35
23	122288	YM	B	L	M	25
24	122288	YM	B	L	M	15
25	122288	YM	B	L	M	5
26	122288	YM	B	L	M	0
27	020789	W	B	0		
28	020889	W	B	0		
29	020889	W	B	S	M	
30	020989	W	B	S	A	
31	021089	W	B	S	F	
32	021089	W	B	0		
33	022189	W	R	0		
34	022289	W	R	S	M	
35	022289	W	R	S	A	
36	022389	W	R	S	F	
37	022389	W	R	0		
38	022789	W	R	0		

MICROBUBBLE EXPERIMENTS

Air Jacket

In the ideal situation, it would be possible to cut the model skin to flush-mount the porous section, as was done in the ARL/PSU geometries. This would cause less disturbance to the flowfield and allow easy installation of a plenum chamber behind the porous sections. However, this would have caused major structural damage to the shell, which was not acceptable as the shell was borrowed from the USNA Crew Team. As a result, it was necessary to design an air jacket in a saddle configuration which would cause minimal alteration to the flow and no alteration to the shell structure.

The air jacket design was conducted with the requirement to provide sufficient structural integrity and flow distribution along its thin section. Generous wax fairing fore and aft of the air jacket was added to help eliminate flow separation.

The midpoint of the air jacket was located 14.5 ft aft of the forward perpendicular on the yellow shell. At this location, the stiffened bulwark around the cockpit was available to secure the air jacket and still remain clear of the force dynamometer and other instrumentation. Data included in Table A2 show that 40 percent of the wetted area of the shell would be downstream of the leading edge of the

air jacket, providing sufficient surface area to measure any significant alteration of the viscous drag by air bubble injection.

The streamwise length of the porous section was chosen at 4.25 in. based on availability of materials as well as air flux considerations. The boundary layer thickness on the model was estimated [Granville, 1959], resulting in a water flow rate of approximately 265 cfm at the highest velocity. At the desired $Q_a/(Q_a+Q_w)$ ratio of 0.3 [Figures 3 and 4], this equates to an air flow rate of 120 cfm. This produced nondimensional air flux (Q/SU) values which were also in the range of ARL/PSU experiments. A nominal filtration grade of 10 microns was chosen. As discussed below, this was expected to give good flow distribution with a pressure drop well within the capacity of the supply system. The basic design of the air jacket was conceived as a sandwich structure with a solid stainless steel backing and a porous stainless steel outer skin [Figures 11].

The lower ends of the two halves of the air jacket were fastened to the centerline skeg of the shell. The upper end of each half was clamped to the cockpit bulwark. The air gaps to allow flow around the entire circumference of the shell were established by three spacers shown in the cutaway view [Figure 12]. The thickness of the porous metal was 0.062 in.

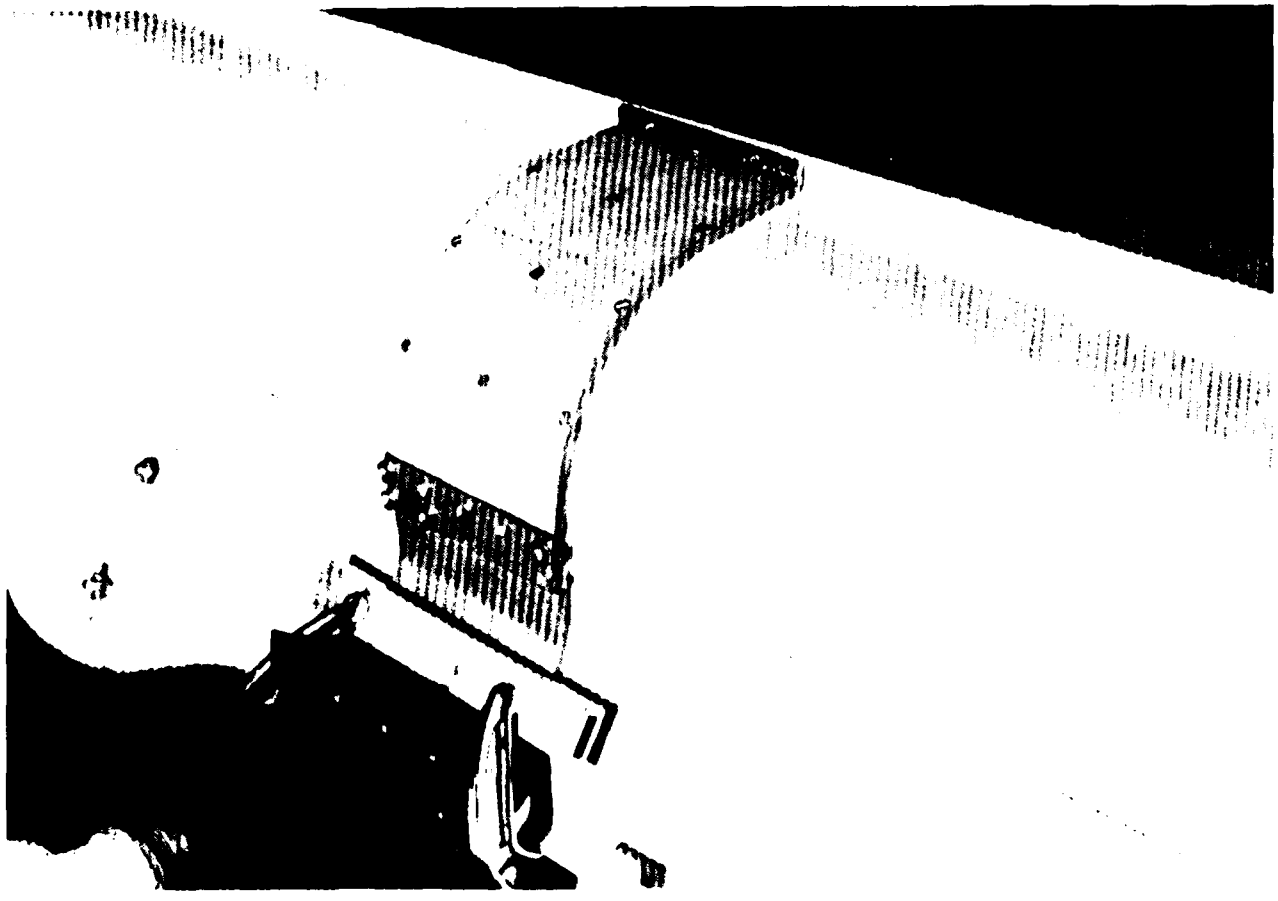

Figure 11a Yellow shell with air jacket (no fairing)

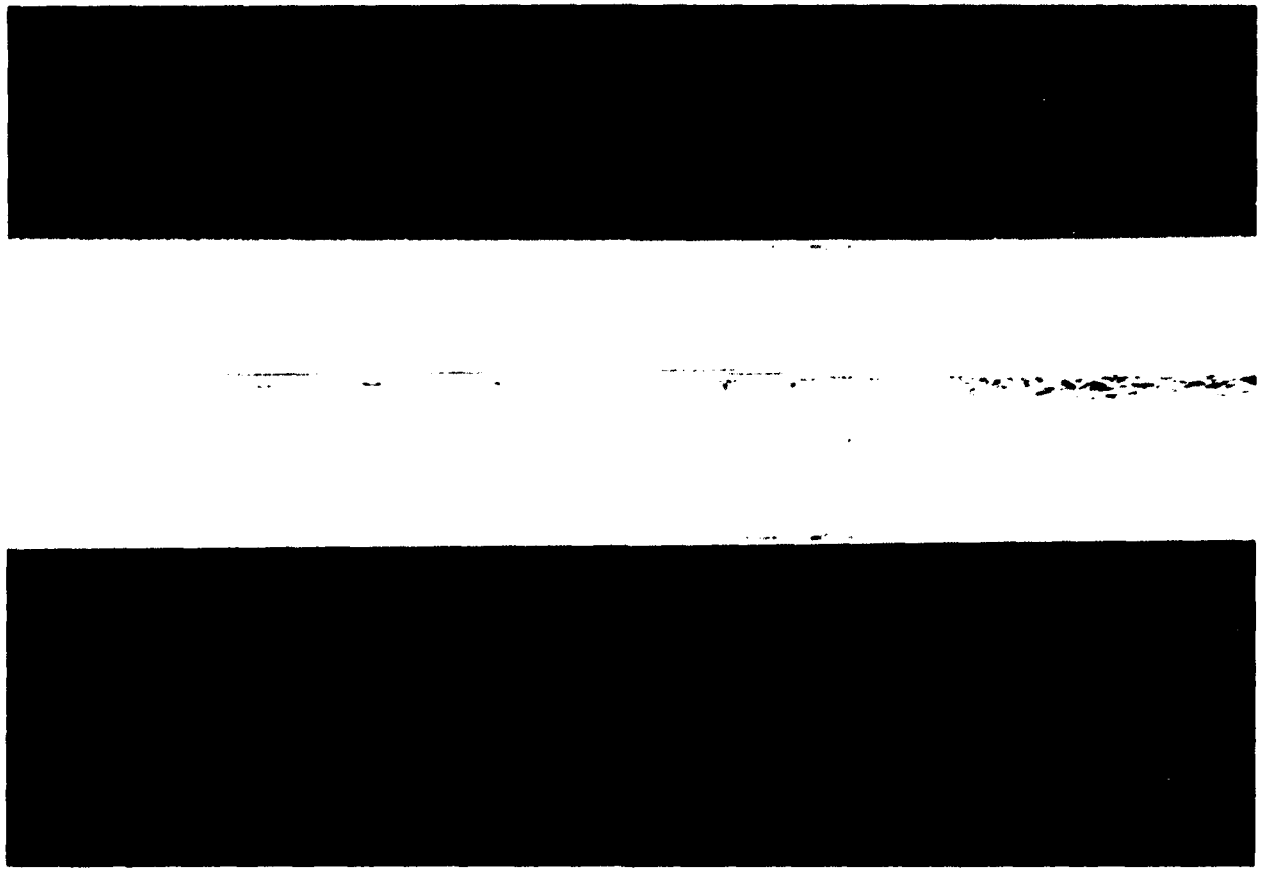

Figure 11b Yellow shell with air jacket (with fairing)

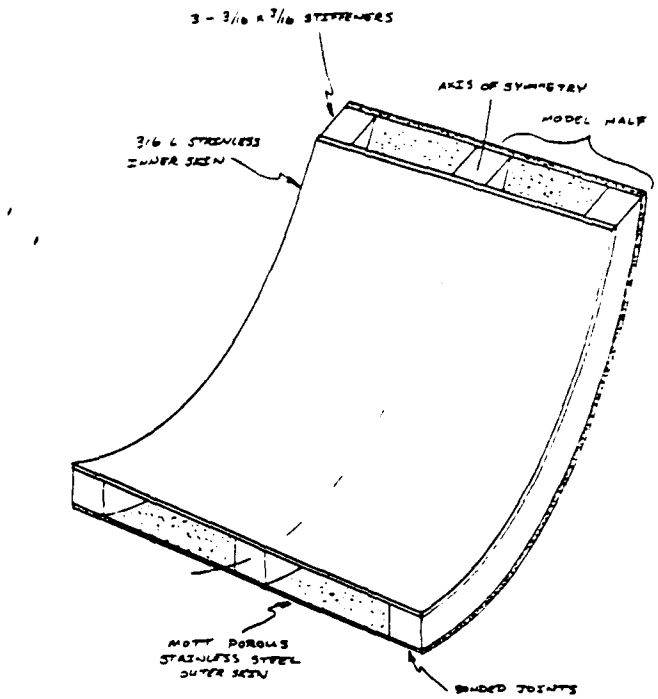

Figure 12 Air jacket (cutaway view)

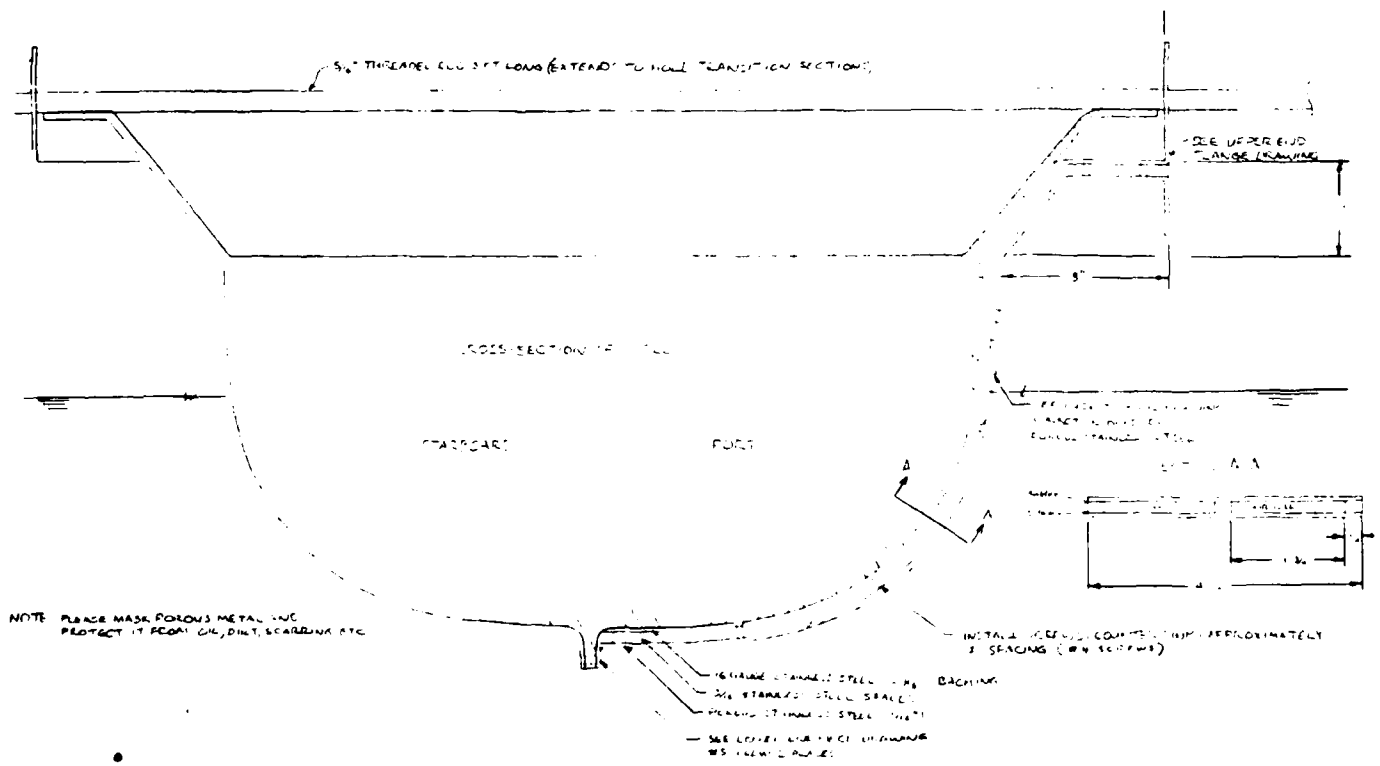

Figure 13 Air jacket with cross-section view

for the standard stock sheets in nominal filter grades of 2, 5, 10, and 20 microns. The solid backing was specified to be 1/16 in. stainless steel to make use of readily available material. With these two thicknesses fixed, the spacer thickness determined the total thickness of the air jacket, which was to be minimized while making the spacer thick enough to provide sufficient stiffness and optimum air flow distribution.

The cross-section of the air jacket is evident from Figure 13. If both skins are assumed firmly pinned to the spacers, then the bending stiffness of the assembly increases approximately as the square of the spacer thickness. This stiffness must counteract the tendency of the structure to straighten out (as a Bourdon tube would) when the internal pressure is applied. The major concerns were the loads applied to the shell by straightening of the air jacket and the buckling loads in the porous side. The porous metal has a stiffness on the order of 10 percent of solid stainless steel (MMC Brochure [1988]).

A finite element analysis of the assembly was performed by Bradel [1988]. The two skins were modelled as rigidly connected plate elements. The internal pressure was calculated for a flow rate of 60 cfm through each side of the air jacket using the manufacturer's data (MMC Brochure

[1988]) for airflow resistance. For 10 micron material, the air flux of approximately 300 cfm/ft resulted in a predicted pressure drop of 1.5 psi. An internal pressure of 10 psi was assumed to provide a sufficient factor of safety in the structural analysis. A spacer thickness of 3/16 in. was used. The analysis was done in two stages. As one case, the air jacket was pinned at one end and not constrained at the other. A deflection of 0.031 in. was computed and considered acceptable. The air jacket was then considered to be pinned at both ends and allowed to transmit loads to the shell solely at those locations. Loads on the order of 20 lbf were computed and considered acceptable, considering that the actual loads would be distributed around the entire

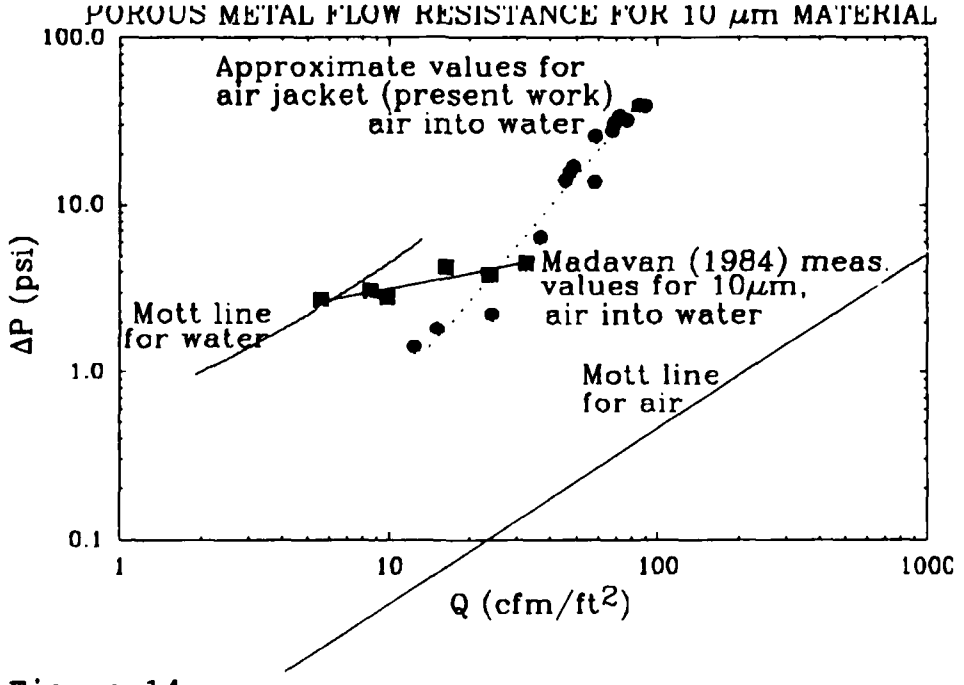

Figure 14

girth. The maximum stress in the porous metal was found to be 27.6 percent of the yield stress.

The validity of the structural analysis was negated by events occurring near the completion of air jacket construction. Most importantly, the calculated resistance of the porous metal [Figure 14] was two orders of magnitude higher in the experimental situation of air flowing into water than would be expected based on the manufacturer's data for air flowing into air. A decision was made to place screws at 2 in. intervals along the outer skin, in order to save time on the tedious process of drilling and tapping small holes (#4) into the stainless steel spacers. The joints between the screw locations were sealed with silicone sealant.

From Figures 12 and 13, it is evident that the air gaps are channels with a length/thickness ratio of 43, so that it is not clear whether or not the outflow would be well distributed. Detailed analysis was undertaken to ensure that the flow rate through the part of the porous wall nearest the skeg would be approximately the same as the flow rate near the inlet. Based on manifold problems involving discrete piping outlets, a good design has high external or outflow resistance relative to the internal resistance along the channel. As in the structural analysis, a large spacer thickness would be desirable, ensuring low internal resistance. In the present case, the design flow rates were such that turbulent flow was

expected inside the air jacket. No general solution for turbulent flow in a porous channel was found in the literature. The laminar flow case has been studied by Berman [1953] and White et al. [1958]. However, it is well known that the internal flow pressure drop is much greater for turbulent flow. Yuan [1959] described a small-perturbation analysis for the turbulent case; however, the analysis requires that axial and outflow velocity profiles be measured in order to complete the solution.

Two numerical approaches were taken to estimate the flow distribution along the air jacket. The first approach, conducted at DTRC, used a simple electrical analogy. A set of 22 nodal equations were written to model the resistance across the porous wall and along the channel. The resistance across the wall was a linear Darcy's Law function using the manufacturer's data for air. The resistance along the channel was determined using the hydraulic diameter and turbulent pipe-flow correlations according to the results given by Hartnett et al. [1962]. A solution was determined by a hand calculation, iterating on the inlet pressure. The second approach, conducted at USNA, used the computer code FLUENT with specially prescribed outflow conditions to simulate the resistance characteristics of the porous metal. The two approaches obtained similar results, namely that the outflow decreased by approximately 10 percent from the top to the

bottom of the air jacket.

As noted earlier, the actual pressure drop across the porous metal after immersion in water was two orders of magnitude higher than expected, and the flow rate achieved was only about one third of the design value. As this indicates much higher outflow resistance and lower internal resistance, the actual flow distribution should be significantly improved over predictions by either analysis.

Air Supply System

The entire air supply system was located on board the carriage in the USNA 380 ft towing tank. Air was supplied from four 30-gallon, 150 psi tanks which were charged by a compressor during the return pass of the carriage. A filter was located between the compressor and the storage tanks. The tank manifold was connected through 30 ft of 1 in. I.D. hose to the metering and control board [Figure 15]. The control elements consisted of a large ball valve (on/off and coarse adjustment), a regulating valve, and various gate valves. The flowmeters consisted of one 2-1/2 in. turbine meter for each side of the air jacket. The flow rates achieved in the experiment were lower than anticipated; therefore, it was necessary to pass the total flow through one of the meters. Flow rates were then approximately matched

Figure 15 Air Flow metering and control board

in the two legs by adjusting the gate valves at the end of the board to equalize the pressure gauge readings. At this point, the air traveled from the control board, at the cabin level of the carriage, through twin 20 ft legs of 3/4 in. I.D. hose to manifolds mounted on the carriage structure above the model. Ten soft neoprene tubes (1/4 in. I.D.) were run to corresponding manifolds on the shell [Figure 16]. Soft tubing having sufficient area to keep the velocity low was chosen in order to prevent transmitting significant restraining forces to the model. As a further preventive measure, a rectangular piece of cardboard was mounted to the carriage immediately forward of the tubing to prevent wind drag on the tubing influencing measured resistance. The air finally passed into 3/4 in. pipe, past a pressure transducer and a temperature transducer, and through 3 ft of hose to each side of the air jacket [Figure 16]. Constant area sheet metal transition sections were constructed to connect 3/4 in. pipe to the highly elongated cross section of the air jacket. Adjustments in the ballasting were made to keep the same waterline as the previous (bare hull) experiments. The weight of the air jacket and manifold setup was found to be less than 5 lbf.

Data were truncated for runs with air flow so that initial and final truncation points enclosed data that had

Figure 16 Shell mounted air supply system

steady air flow rate and steady velocity. At the higher air flow rates, the ball valve had to be opened at the proper time as the carriage accelerated in order that the two conditions coincide for the maximum possible time. The manufacturer's flowmeter calibration was used. In addition, the meter was used well below its recommended minimum flow rate of 22 cfm (as low as 5 cfm), so that some nonlinearity probably occurred in this range. No corrections for temperature or pressure were made. At the highest air flow rate, a temperature decrease of 0.5 deg C of the air was observed during a complete discharge of the tanks.

Zero speed measurements were recorded for each flow rate, in order to account for buoyancy effects and the minor effects of tubing deflections that could bias drag readings. Small negative values of drag were recorded and used as offsets (considered constant over speed range) to correct forward-velocity drag measurements for each flow rate.

EXPERIMENTAL DATA ANALYSIS

MATHEMATICAL MODEL

In order to analyze the data from the riblet and microbubble experiments and to isolate the effects of adding riblets, air injection, and a trip wire, certain assumptions were made and a mathematical model formulated. The major components of fluid mechanical drag on a marine vehicle are shear or viscous drag which is primarily a function of Reynolds number (R_n), pressure and wave drag which are primarily functions of Froude number (F_n), and surface tension which is primarily a function of Weber number (W_e). The effect of surface tension is considered to be negligible for surface models with length greater than 5 ft. For the purposes of this analysis, air resistance was assumed to be negligible. As a result, the total resistance coefficient may be expressed as follows:

$$C_T\ (R_n,\ F_n) = C_F\ (R_n,\ {\sim}F_n) + C_R\ (F_n,\ {\sim}R_n)$$

where ~F_n refers to the weak interaction between Froude number and friction resistance caused by changes in the wetted surface area, and ~R_n refers to the weak interaction between

Reynolds number and residual resistance due to the boundary layer thickness altering the effective size and shape of the body. Based on Froude's hypothesis (Comstock, [1967] or Gillmer and Johnson [1982]) these weak interactions are neglected and the following simplification used:

$$C_T\ (R_n,\ F_n) = C_F\ (R_n) + C_R\ (F_n)$$

This results in an extremely tractable algorithm which has been used in ship resistance analysis for design purposes since the turn of the century. While acceptable for overall ship power prediction, this simplification may be too crude to account for microscopic surface phenomena such as riblets or microbubbles. Nevertheless, as a starting point, this simplifying assumption of resistance component separability was adopted.

Based on the various configurations tested, this model was further broken down to the individual C_F and C_T components contributed by the addition of riblets and a trip wire, respectively:

$$C_T = (C_F)_{ITTC} + (\Delta C_F)_{RIB} + C_{RO} + (\Delta C_T)_{TRIP}$$

In all cases, coefficients were calculated by comparing faired plots (obtained through regression analysis) of the

actual data points which will be discussed at length in the following paragraphs.

$(C_F)_{ITTC}$ represents the turbulent skin friction coefficient for the baseline condition (bare hull) (assumed be the ITTC value from Comstock, 1967) as shown below:

$$(C_F)_{ITTC} = 0.075/(\log_{10}R_n - 2)^2$$

C_{RO} and C_{RO}^* represent the residual coefficient for the baseline conditions, bare hull or bare hull with trip, respectively, and were calculated as follows:

$$C_{RO} = C_{TO} - (C_F)_{ITTC} \quad \text{for bare hull}$$

$$C_{RO}^* = C_{TO}^* - (C_F)_{ITTC} \quad \text{for bare hull with trip}$$

These residual coefficients include form drag and wave making resistance coefficients.

$(\Delta C_F)_{RIB}$ was the change in skin friction coefficient caused by the addition of riblets to the bare hull or bare hull with trip wire configurations. As riblets reduce turbulent skin friction drag, both situations were studied to determine the difference in drag reduction between allowing "natural" transition in the bare hull case and forcing transition in the trip wire case. Any wavemaking effects, ($(\Delta C_R)_{RIB}$), were considered to be negligible. The friction

drag effect was isolated by removing the residual drag of the baseline condition, C_{R0} or C_{R0}^{*}, from the total resistance with the riblets:

$$(\Delta C_F)_{RIB} = ((C_T)_{riblets} - C_{R0}) - (C_F)_{ITTC}$$

or

$$(\Delta C_F)_{RIB} = ((C_T)_{riblets} - C_{R0}^{*}) - (C_F)_{ITTC}$$

This result was then compared with $(C_F)_{ITTC}$.

The effect of the trip wire would typically be manifested almost solely as an increase in residual coefficient, a major portion of which is due to the parasite drag of the trip (a R_n dependent effect) and, to a lesser extent, the wavemaking drag of the trip (a F_n based effect). Another possible effect is an alteration in the frictional resistance due to changes in wetted surface area caused by venting of the trip wire. The total effect was isolated by comparing the total resistance coefficients of the bare hull with trip wire to that without in the following manner:

$$(\Delta C_T)_{TRIP} = (C_T)_{TRIP} - (C_T)_{NOTRIP}$$

For comparison, a theoretical $(C_T)_{TRIP}$ (assuming the $F_n = 0$ waterline) was calculated in the following manner:

$$(\Delta C_T)_{TRIP} = (D * g_{tw}/S) * C_D$$

C_D is based on Koslov's formula (see Koslov [1969]) for the drag on a trip wire:

$$C_D = 2.6/(R_k)^{1/2} + 0.6$$

This predicted result was then compared with the experimental data.

The model was also broken down to the individual C_T components contributed by the addition of the air jacket and air injection, respectively:

$$C_T = (C_F)_{ITTC} + C_{R0} + (\Delta C_T)_{AJ} + (\Delta C_T)_{BLOW}$$

$(\Delta C_T)_{AJ}$ represents the increase in the total resistance coefficient due to the addition of the air jacket, determined as follows:

$$(\ C_T)_{AJ} = (C_T)_{AJ} - C_{T0}$$

The effect of the air jacket is primarily one of increased residual drag (a F_n effect) due to the addition of a section of increased beam and draft near midships. The addition of fairing [Figure 11b] tends to minimize the residual drag but also introduces a frictional effect by

increasing the wetted surface area (a R_n effect). No attempt was made to further isolate these effects.

$(\Delta C_T)_{BLOW}$ represents the change in the total resistance coefficient due to air injection. This effect was isolated by comparing the results at each flow rate with those for no flow as follows:

$$(\Delta C_T)_{BLOW} = (C_T)_Q - (C_T)_{Q=0}$$

RIBLET EXPERIMENTS

The results of the riblet experiments that follow were obtained from faired plots [Figure 17]. The wave drag at low F_n would be expected to approach zero, leading to a condition where C_{R0} consists entirely of form drag. This form drag may be attributed to pressure recovery losses due to boundary layer development. At this point, it is seen that the form drag is approximately 4 percent of the friction drag and the total resistance at near-zero Froude numbers may be described by multiplying $(C_F)_{ITTC}$ by the Hughes form factor of r = 1.04 [Comstock,1967,p. 300]. This factor may be extrapolated across the Reynolds number range as the total "viscous" resistance. A simpler model is to assume the form drag coefficient (C_{FORM}) to be constant over the Reynolds number range and to determine the total "viscous" resistance by adding this offset to the value of $(C_F)_{ITTC}$. In either case, subtracting this total viscous resistance from the total resistance should produce the wavemaking resistance. In the data analysis, the difference between the total resistance coefficients for different conditions was sufficient to isolate the individual effects. As a result, values for C_T were compared directly or the offset accounted for by inclusion in C_{R0}.

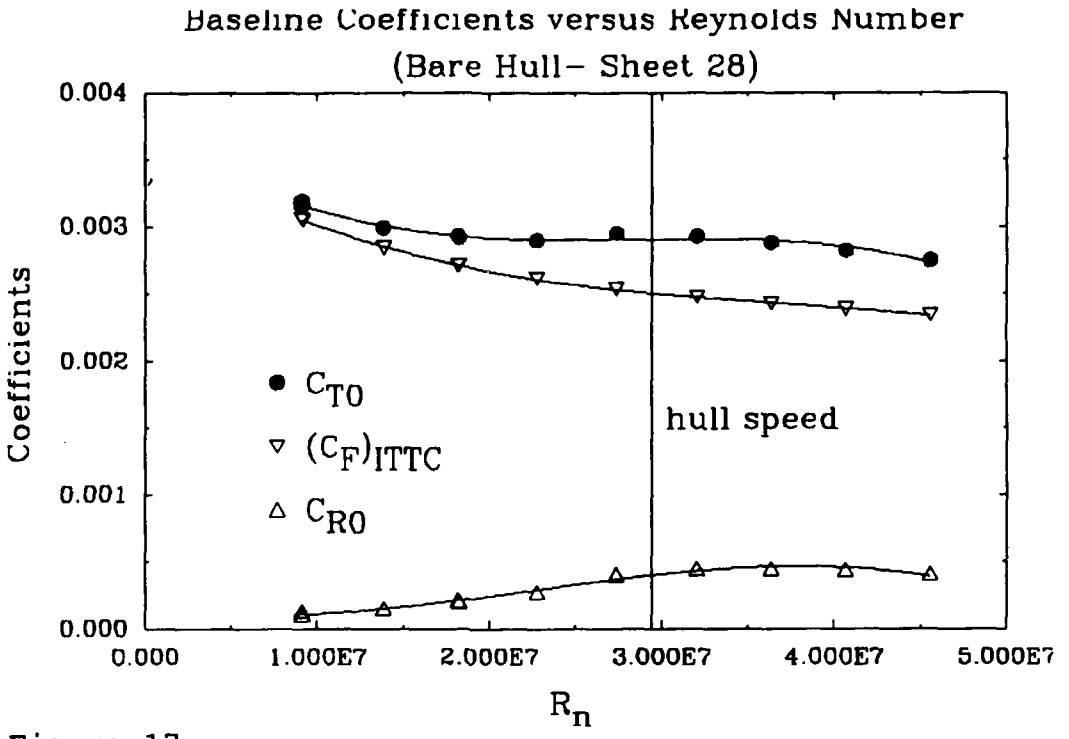

Figure 17

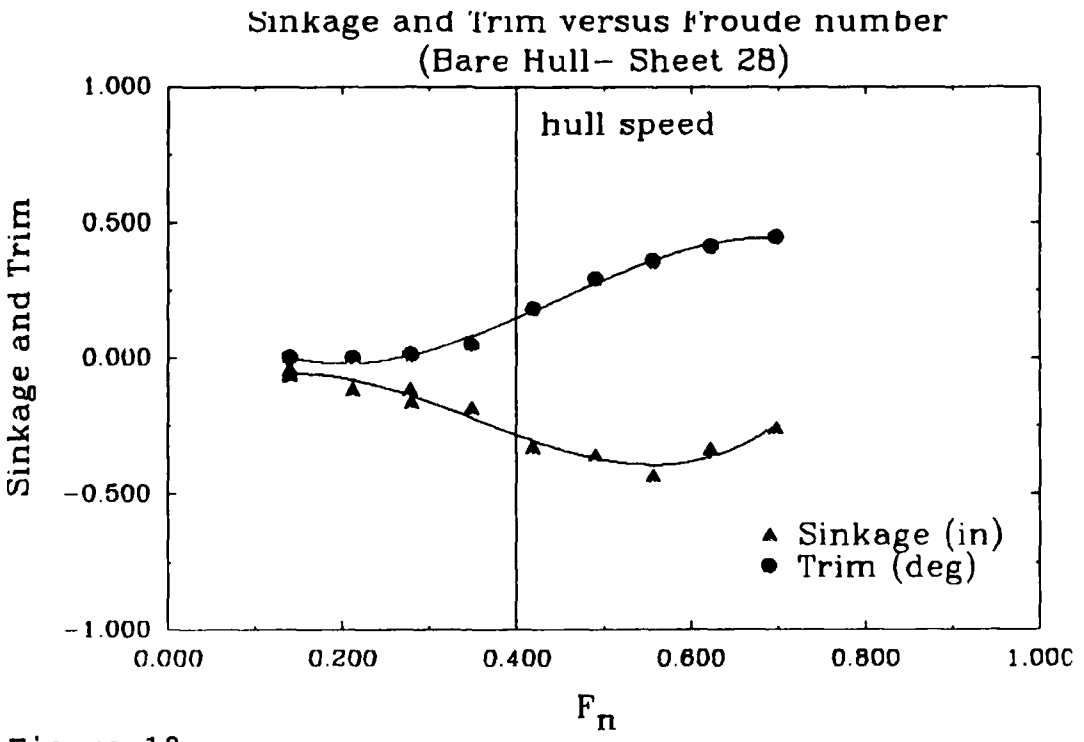

Figure 18

Wave resistance becomes a significant factor when the wave length is on the order of the ship length. The speed at which this occurs is called the hull speed and is the point at which $F_n = 0.4$, correlating to a velocity of 11.5 ft/sec ($R_n = 2.94 \times 10^7$) for the white shell. For higher velocities, the distance between waves exceeds the length of the hull, causing an increase in both sinkage and trim [Figure 18] as the stern of the model falls into the trough of the bow wave.

The effects of riblets were analyzed under conditions where transition was allowed to occur "naturally" (bare hull) as well as for the case where transition was induced by a trip wire. These results are shown in Figures 19 and 20, respectively. The bare hull results include the tests conducted by McKelvey in 1988 and show the repeatability of the drag reduction which averaged approximately 3 to 3.5 percent over the higher range of velocities (greater than 10 ft/sec). At the lower velocities, there was significant scatter and some drag increases in the results, which may be attributed to the unpredictability of transition. For the low speed runs, there were sizeable differences in the measured resistance between runs conducted when turbulence in the tank was relatively low (at the beginning of the day or after long periods between runs) and runs when turbulence was higher (following high speed runs). The greatest resistance

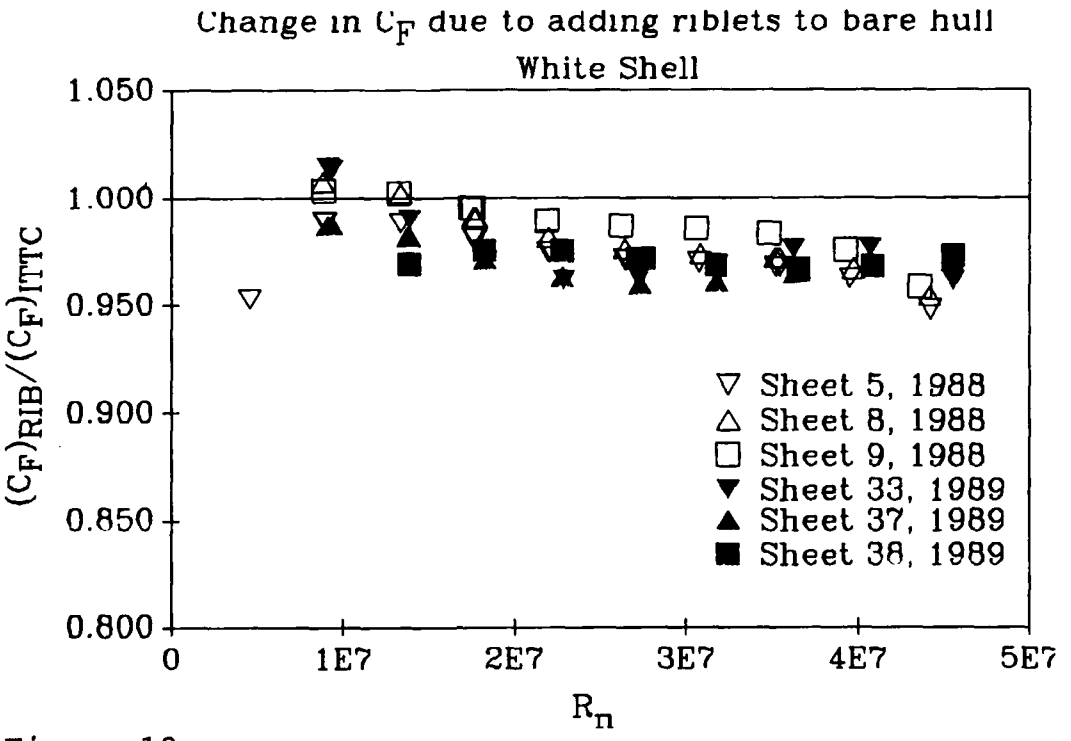

Figure 19

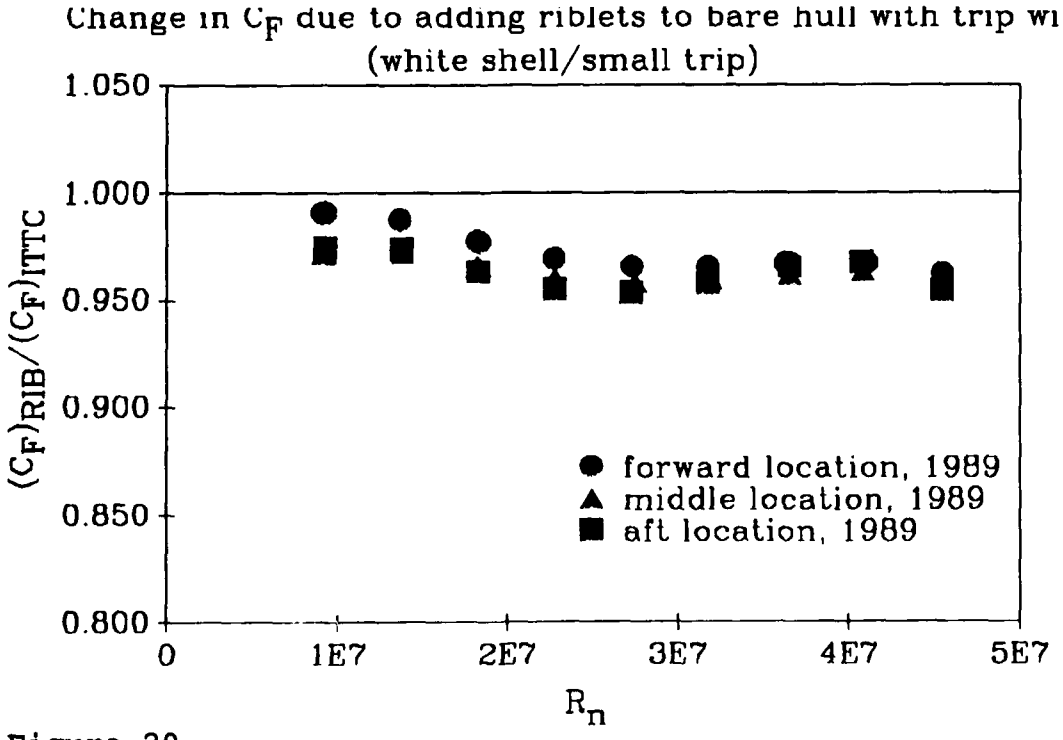

Figure 20

change was measured when the residual turbulence was high. As the drag reduction capabilities of riblets depend on the presence of turbulent flow, this may be attributed to residual turbulence in the tank "tripping" transition to turbulent flow on the shell. A similar "tripping" effect may have been caused at the lower speeds by vibration of the towing carriage.

These low speed effects provided motivation for the trip wire experiments. Sample results are presented in Figure 20. As expected, the trip wire data showed considerably less scatter over the range of velocities. The location of the trip wire appeared to have minimal effect (at the highest Reynolds numbers) on the measurable drag with the addition of riblets. The significantly reduced scatter at the lower velocities tends to support the possibility of ambient turbulence or vibration induced transition and indicates the necessity of a reliable means of fixing the point of transition. Further investigation of these effects was conducted by measuring carriage vibration and turbulence in the tank at the end of the testing period (Sheets 37 and 38). The results of these studies will be reported in a later publication.

In addition, the effect of adding a trip wire to the bare hull configuration was studied at length. The results for these studies are shown in Figures 21. For comparison,

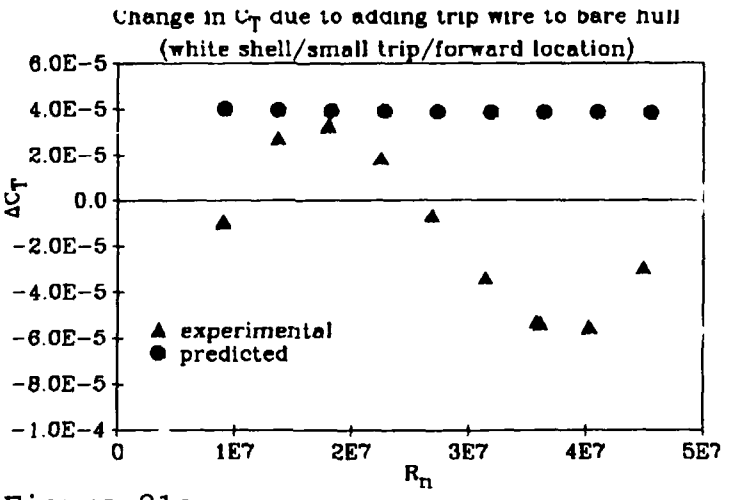

Figure 21a

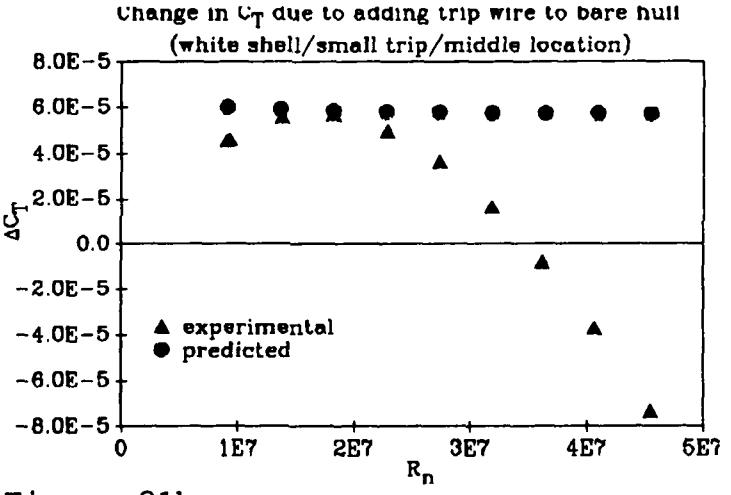

Figure 21b

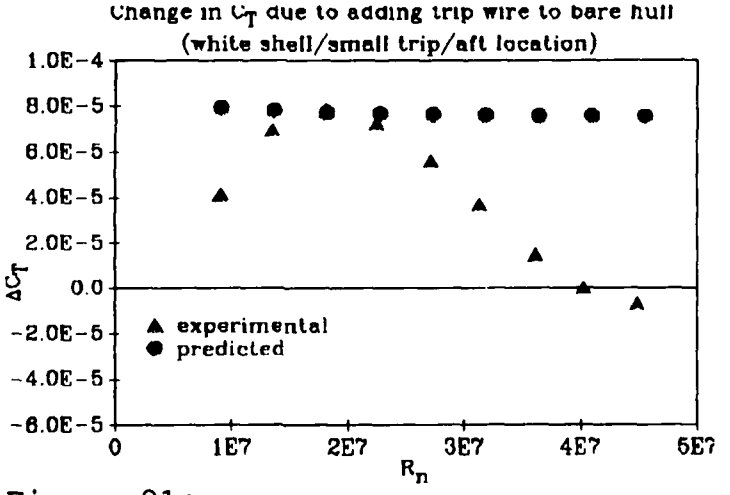

Figure 21c

the predicted change in total resistance coefficient due to trip wire parasite drag, $(\Delta C_T)_{TRIP}$, is presented with the experimental results. In the case of the small trip wire, the experimental results show significantly less resistance than theory at the extremes of velocity. The low velocity results may be attributed to the transition effects previously discussed as well as experimental scatter. The theoretical results are based on the zero Froude number waterline, assuming that both the wetted surface area of the shell and the wetted girth of the trip wire are constant. Due to the increase in sinkage and trim when the hull speed is exceeded, both the wetted girth and surface area are significantly changed, which probably accounts for some of the discrepancy. There is, however, a measured drag reduction for higher velocities. This may be a true hydrodynamic effect or possibly a test anomaly having to do with the tow point geometry and the coupling between pitch, heave, and lift. The spray pattern with the trip wire is observably different from that of the bare hull and the trip wire ventilates down to the skeg for some conditions. The trip wire vent [Figure 22] changes the wetted surface which could lead to a drag reduction. In addition, the pressure distribution of the hull is altered. The causes of this apparent drag reduction that increases with velocity are difficult to ascertain.

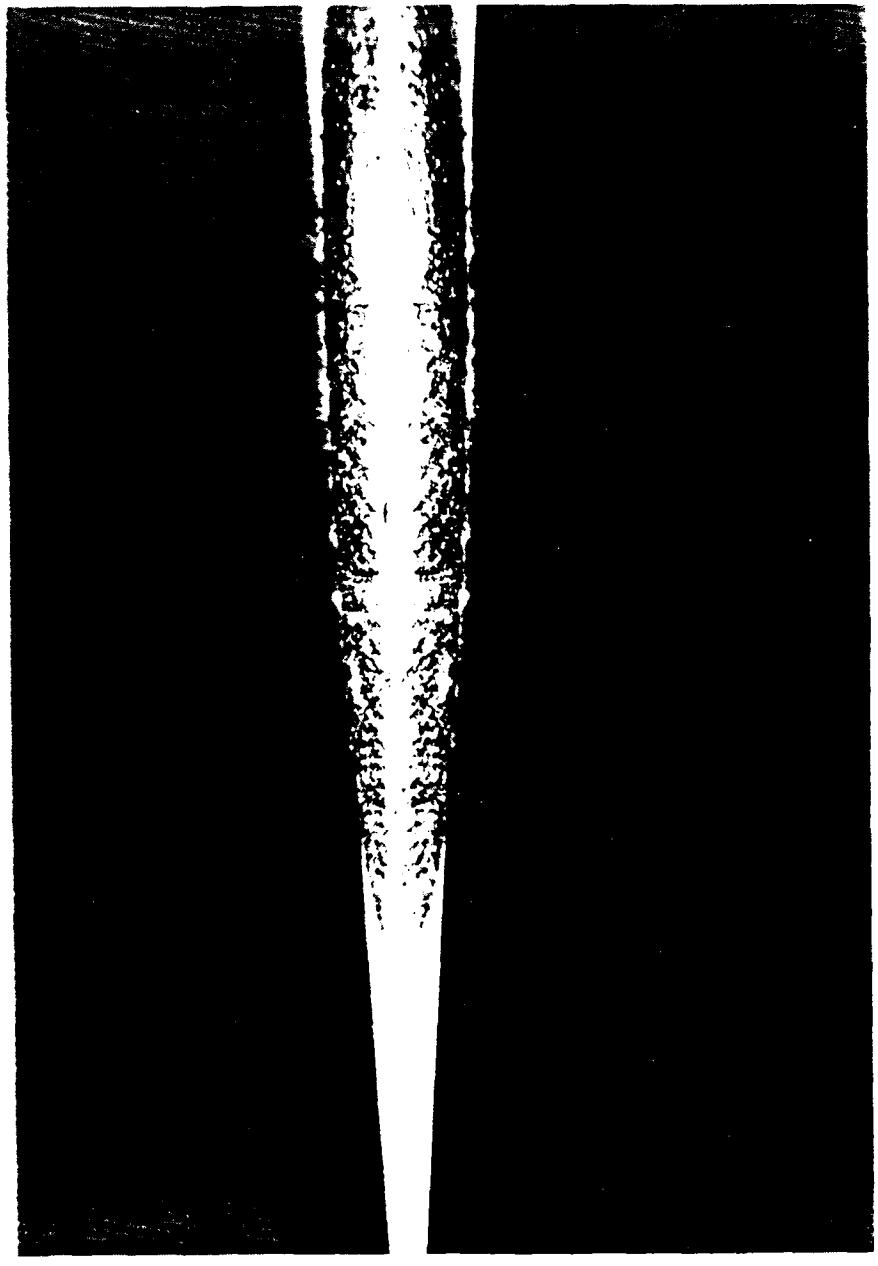

Figure 22 Underwater view of trip wire venting

The combined effects for the addition of both riblets and trip wire to the bare hull are presented in Figures 23. In order to gain some insight into the interaction between the drag reduction mechanisms of riblets and trip wires, the sum of the separate effects ($(\Delta C_F)_{RIB} + (\Delta C_T)_{TRIP}$) of adding riblets to the bare hull and trip wire to the bare hull was plotted along with the total effect of the two devices applied together($(\Delta C_T)_{RIB+TRIP}$). It is evident from Figures 23 that drag was consistently reduced over the range of speeds with the maximum reduction of about 6 percent occurring at the highest speeds with the trip wire in the middle position. It should be noted that this position corresponds with the beginning of the riblet tape. As the usefulness of riblets depends on turbulence, it would seem logical that the middle location would be the most desirable, as it ensures turbulent flow over the entire riblet surface without sacrificing any additional turbulent drag penalties over the region forward of the riblets. This would be expected from the riblet and trip wire results taken individually. The riblets developed a fairly consistent drag reduction across the speed range while the trip wire results generally showed drag increases at the lowest speeds and modest drag reduction in the higher speed range which increased with velocity. Further study into the optimum trip wire/riblet configuration will be conducted at

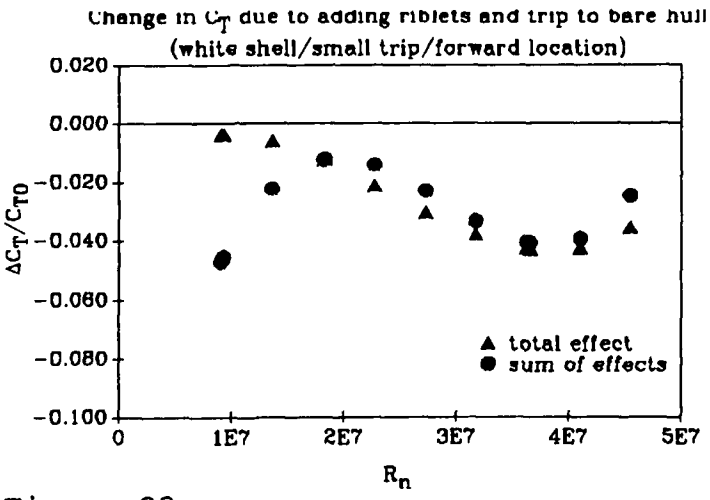

Figure 23a

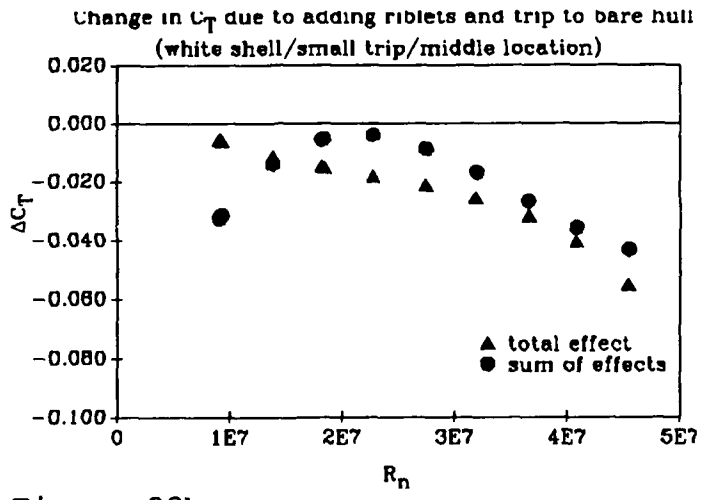

Figure 23b

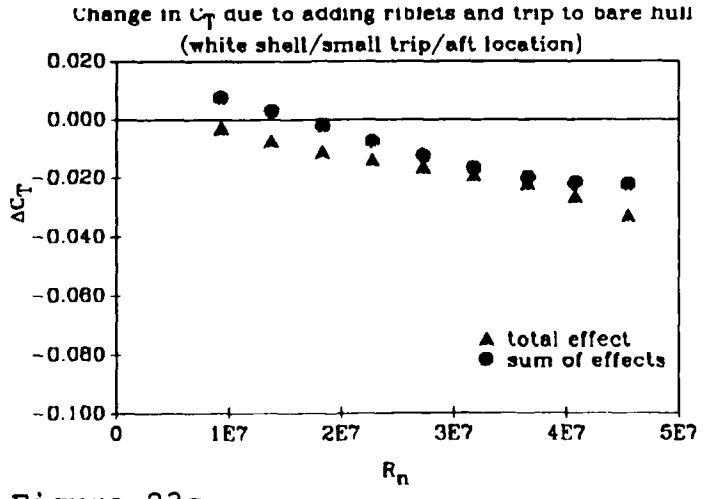

Figure 23c

DTRC (see Coder et al. [1989]).

For all of the trip wire locations, the sum of the effects followed some interesting trends. At the lowest velocities, the sum and the total are seen to differ markedly. These differences may once again be attributed to the instability of transition in this velocity range and the fact that these results are based on comparisons between runs in which ambient turbulence and vibration are not well documented. At the higher velocities ($R_n > 1.8 \times 10^7$), Figures 23 indicate that the combination of trip wire and riblet effects are approximately additive but that the sum of effects shows consistently less drag reduction with the difference increasing with speed. This may be considered a result of small destructive interactions between the riblets and trip wire.

MICROBUBBLE EXPERIMENTS

Performance of Air Jacket

The air jacket did not perform as expected. Its performance is relevant, however, in that it affects interpretation of the drag results, provides information for further experiments, and raises some interesting questions about the mechanisms of bubble formation.

The air jacket was connected to the air supply system on shore for preliminary testing. The pressures were relatively low, on the order of 1 psi, as expected from the manufacturer's data [Figure 14]. However, upon immersion the back pressure increased considerably, the increase persisting after the air jacket was removed from the water. The resistance of the porous metal during the actual experiments was approximated using the pressure transducer data. These results are shown in Figure 14, with the manufacturer's data shown for air and water. Data from the dissertation by Madavan [1984] also became available after the experiment and are included in Figure 14. These data lead to the conclusion that air flowing into water (or air flowing through wetted media) requires a driving pressure two orders of magnitude higher than air alone. Surface tension acting on the air as bubbles are created on the exterior of the jacket is only

sufficient to explain approximately 5 psi, with reasonable assumptions on bubble size. It is also interesting to note that Madavan's other data (not shown) indicate no significant difference in pressure drop for pore sizes varying from 10 to 100 microns.

The high pressure drop had several effects on the experiment. As the supply (storage tank) pressure was fixed, the achievable flow rate was reduced to approximately 40 cfm (the design flow rate was 120 cfm total), resulting in use of the flowmeter below its design range. In contrast, a beneficial side-effect of higher resistance would be improvement of flow distribution. The air jacket was observed with mirrors from the lower carriage platform and the air appeared to be emerging from the full girth of the model in a uniform manner.

A major result of the high airflow resistance was increased structural loads on the air jacket. As shown in Figure 14, pressures of 40 psi were reached at the highest flow rate. The sequence of flow rates tested is illustrated in Figure 24. The air flow rate was gradually increased on Days 1 and 2. When the highest flow rate (37 cfm) was reached, a whistling tone was heard in the area of the apparatus. Various connections were checked and tightened without correcting the discrepancy. Intermediate flow rates

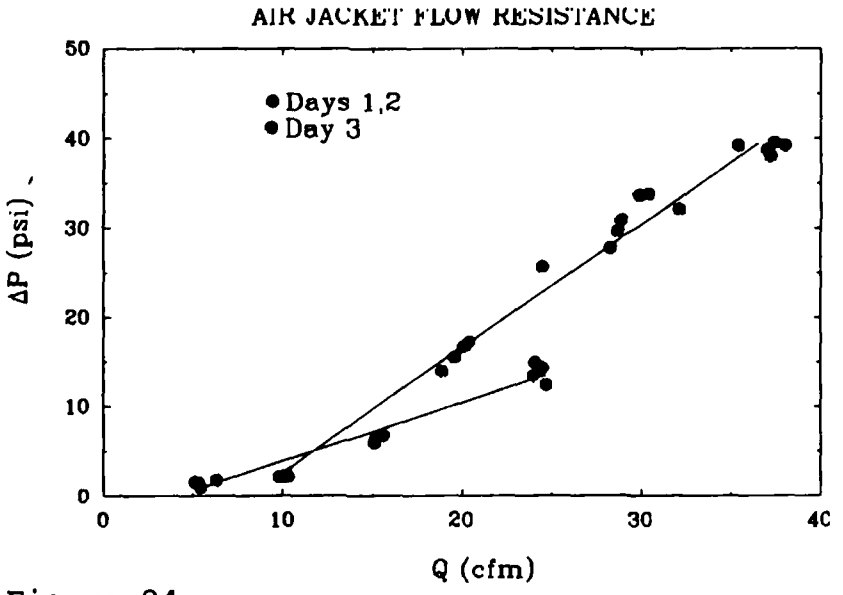

Figure 24

were tested on Day 3, as shown in Figure 24, to complete the experimental matrix. From the trends shown in this figure, it appears that the total resistance characteristic of the system (the quantity actually measured by the pressure transducer) was different for Day 3 than Days 1 and 2. Possible explanations for this phenomenon include a failure in the silicone sealant, or buckling of the porous metal between the screws securing the outer skin of the air jacket, although none was observed.

Total Drag Results

The raw drag data registered by the force block are first considered. Figure 25 shows the total envelope of measurements, from Q=0 to Qmax 37 cfm, with total hull

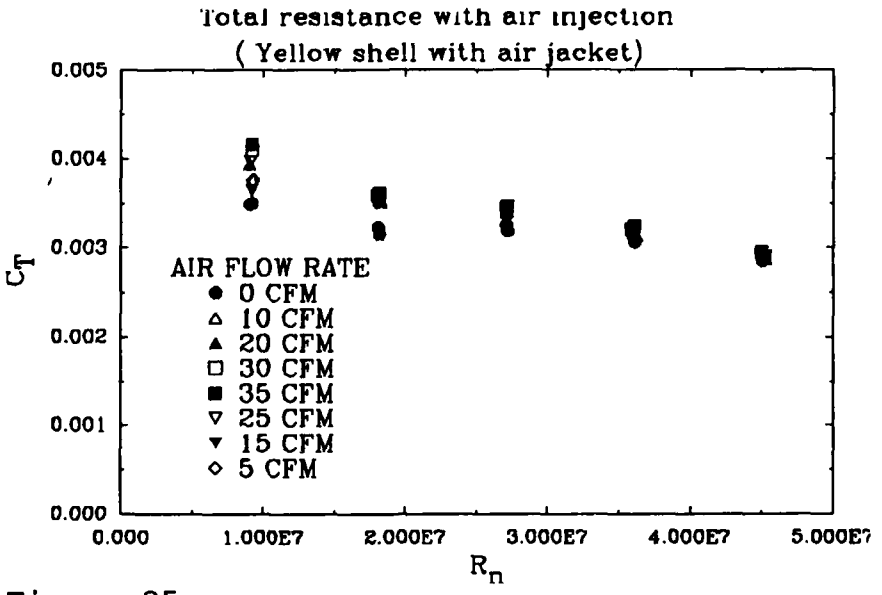

Figure 25

resistance, C_T, increasing with increasing flow rate. In order to isolate the effect of air injection from that of the air jacket, two baseline (Q = 0) tests were conducted. These were the first and last data sets conducted during the three days of air jacket experiments. In Figure 26, these

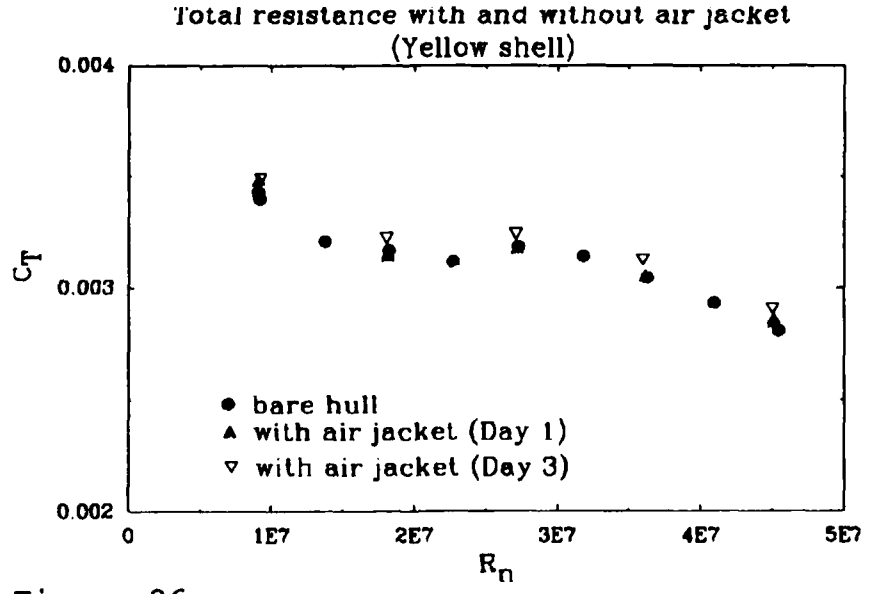

Figure 26

baseline tests are compared with the bare hull condition to give some insight into the relative magnitude of the air jacket effects. These effects may be considered a result of wavemaking or form drag induced by increasing the effective size of the body. These results are represented as the change in total resistance caused by air injection [Figure 27]. Minimal reduction in total drag was observed for the highest speed (20 ft/sec) and flow rates (30 and 35 cfm) and drag increases were evident for all other conditions. It should be noted that for a fixed air flow rate, the drag ratio decreases, approaching unity as the speed is increased. The scatter at the lowest speeds is representative of the proportionally large uncertainty at these speeds.

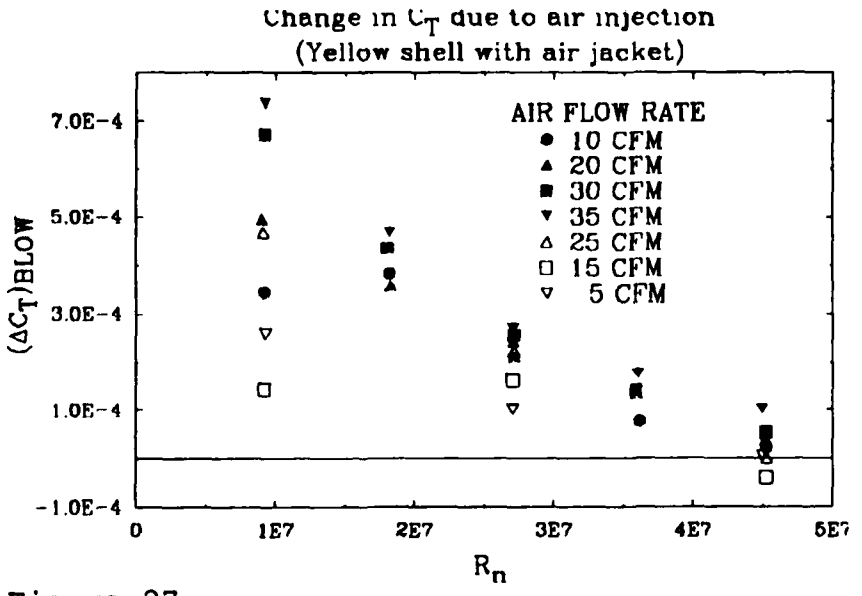

Figure 27

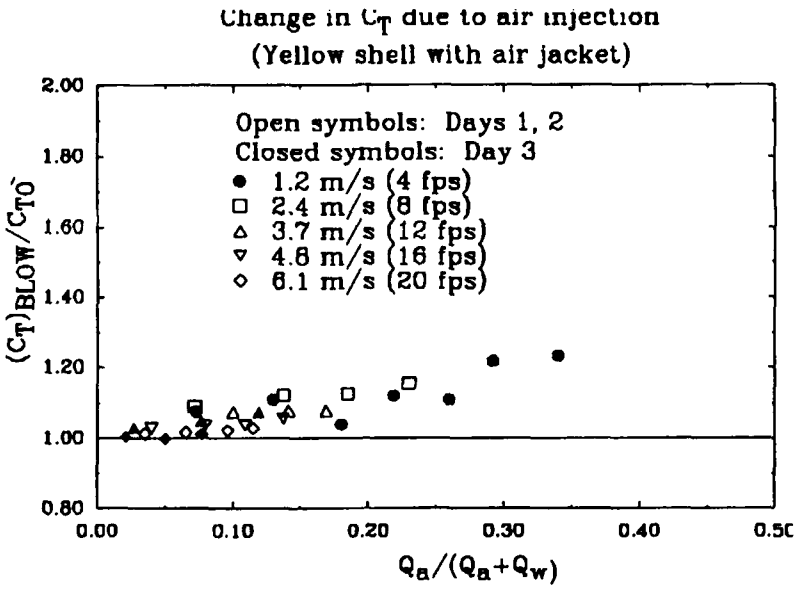

Figure 28

The normalized results are presented in Figure 28, with boundary layer thicknesses estimated from Granville's [1959] correlation, with a turbulent boundary layer assumed to begin at the forward perpendicular. Refinements of this estimate are possible and should produce small shifts in the relative results. At the design speed of 20 ft/s, a normalized flow rate of well below the design value of 0.3 was achieved as a result of the unexpectedly high resistance of the porous metal.

Drag increases of up to 23 percent were measured in the present experiments, which were conducted on a surface model and at a lower speed range than the ARL/PSU work. In addition to these factors, there are other physical differences. The model was free to move about the towing point, while the area covered by air emission was not

symmetric about the tow point. Subsequently, changes in wetted area due to pitch and heave changes were possible. It may be feasible to isolate the C_F and C_R components of the drag; however, such analyses were considered beyond the scope of this report.

Visual Evidence

Photographs taken from the port side of the model, below the free surface, are shown in Figures 29-32. The shell is moving from right to left in all photos. Only the lower half of the picture should be considered as the upper half is a reflection of the underwater portion of the shell on the free surface. A shutter speed of 1/250 second was used. Only at the highest speeds and relatively low flow rates was a cloud of apparently small bubbles ("microbubbles") observed. At the lowest speed and highest air flow rate [Figure 29] the air appears to have coalesced into a single, large volume. For moderate speed and flow rate, there appears to be small bubble creation but separation seems to occur within a limited distance from the point of air injection. At the highest speed and low-to-moderate flow rate (Figures 31) the cloud of bubbles would be expected to remain attached to the hull for a considerable distance. At the highest speed and flow rate,

Figure 29 Air injection (U = 4 ft/sec, Q = 37 cfm)

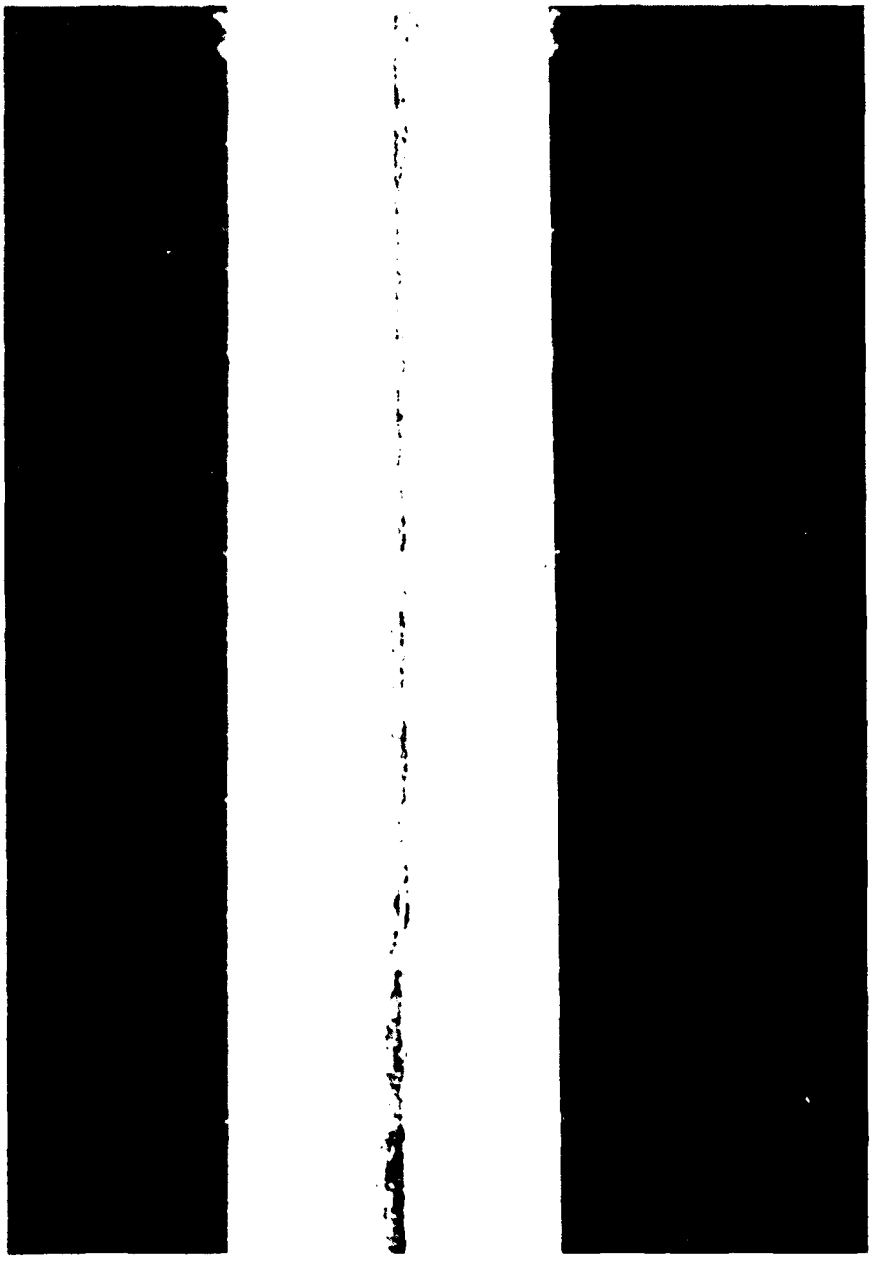

Figure 30 Air injection (U = 12 ft/sec, Q = 5 cfm)

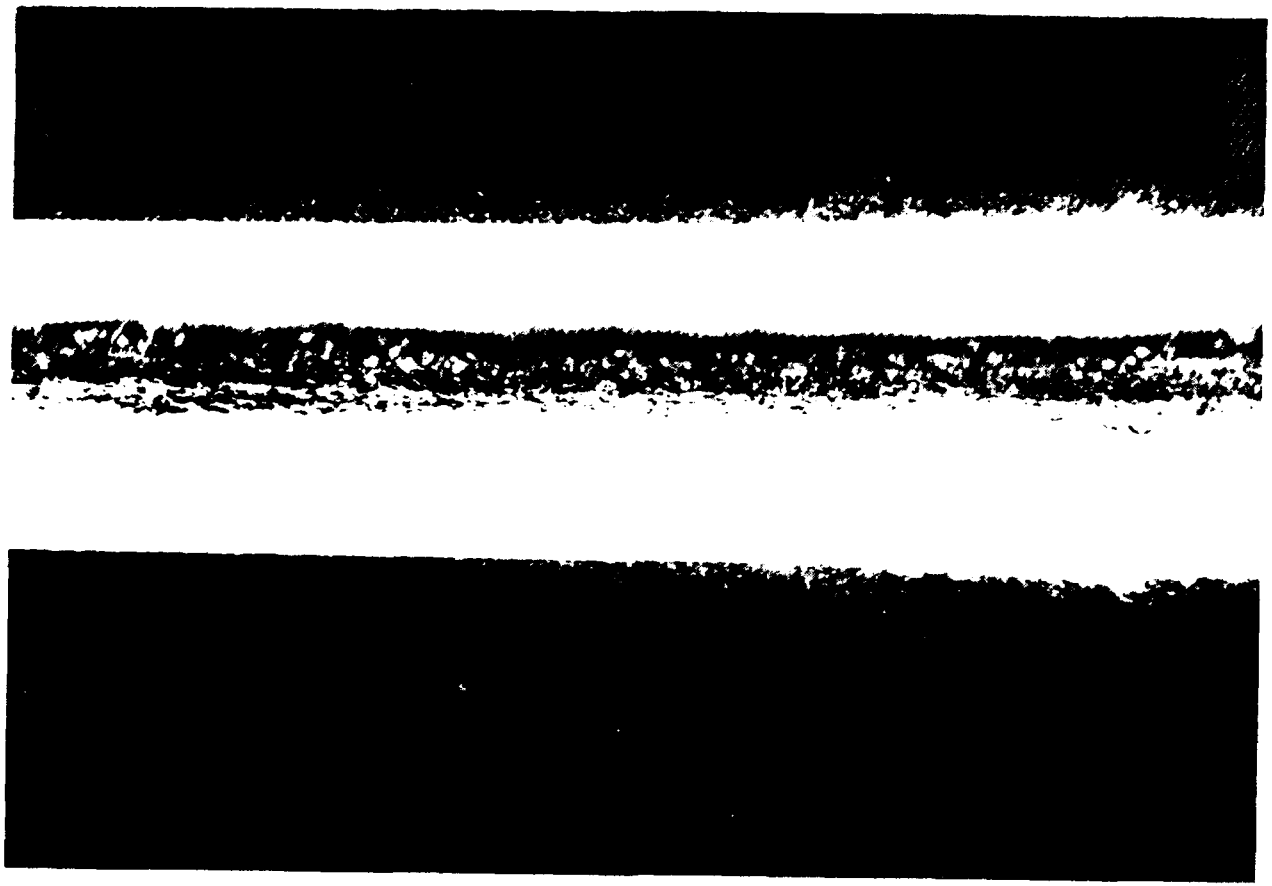

Figure 31 Air injection (U= 20 ft/sec, Q = 15 cfm)

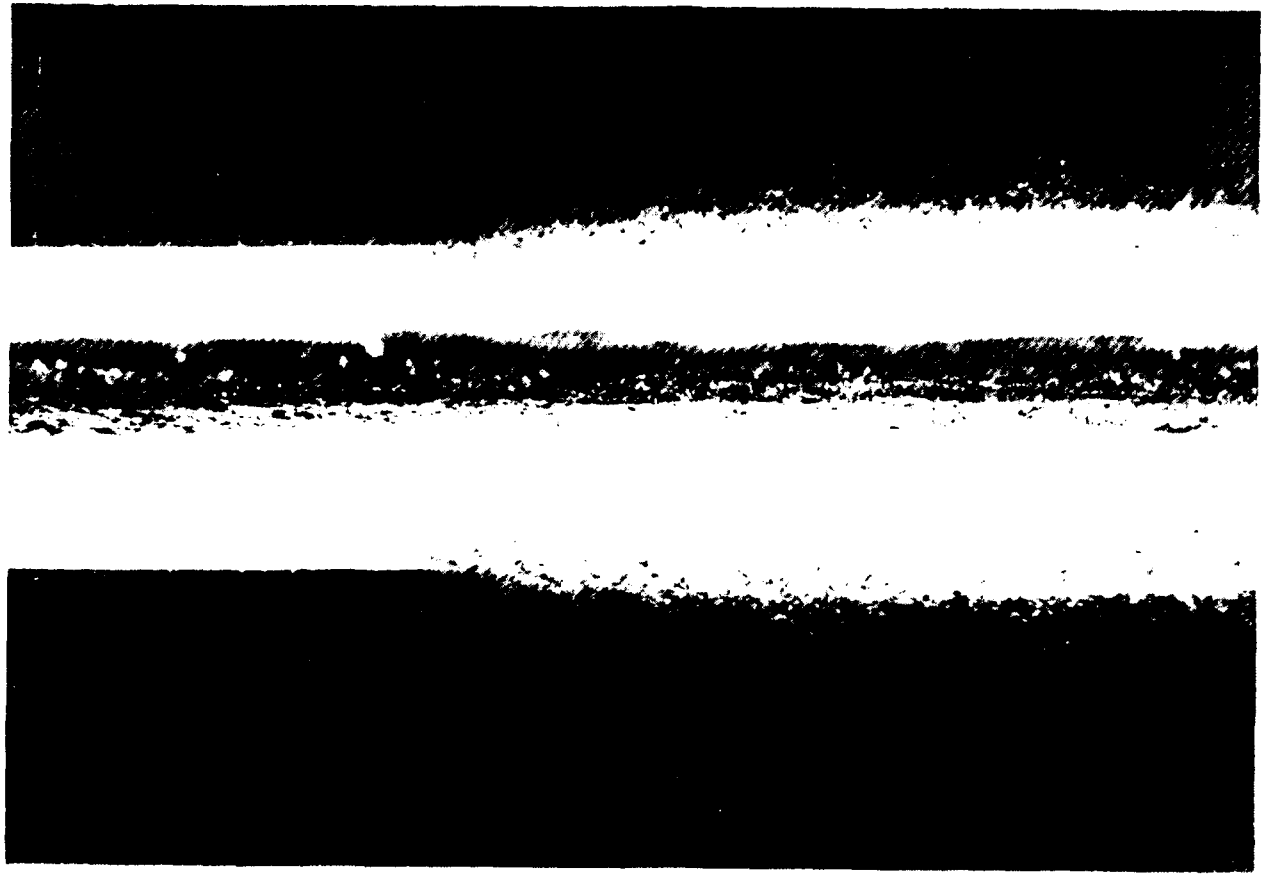

Figure 32 Air injection (U = 20 ft/sec, Q = 37 cfm)

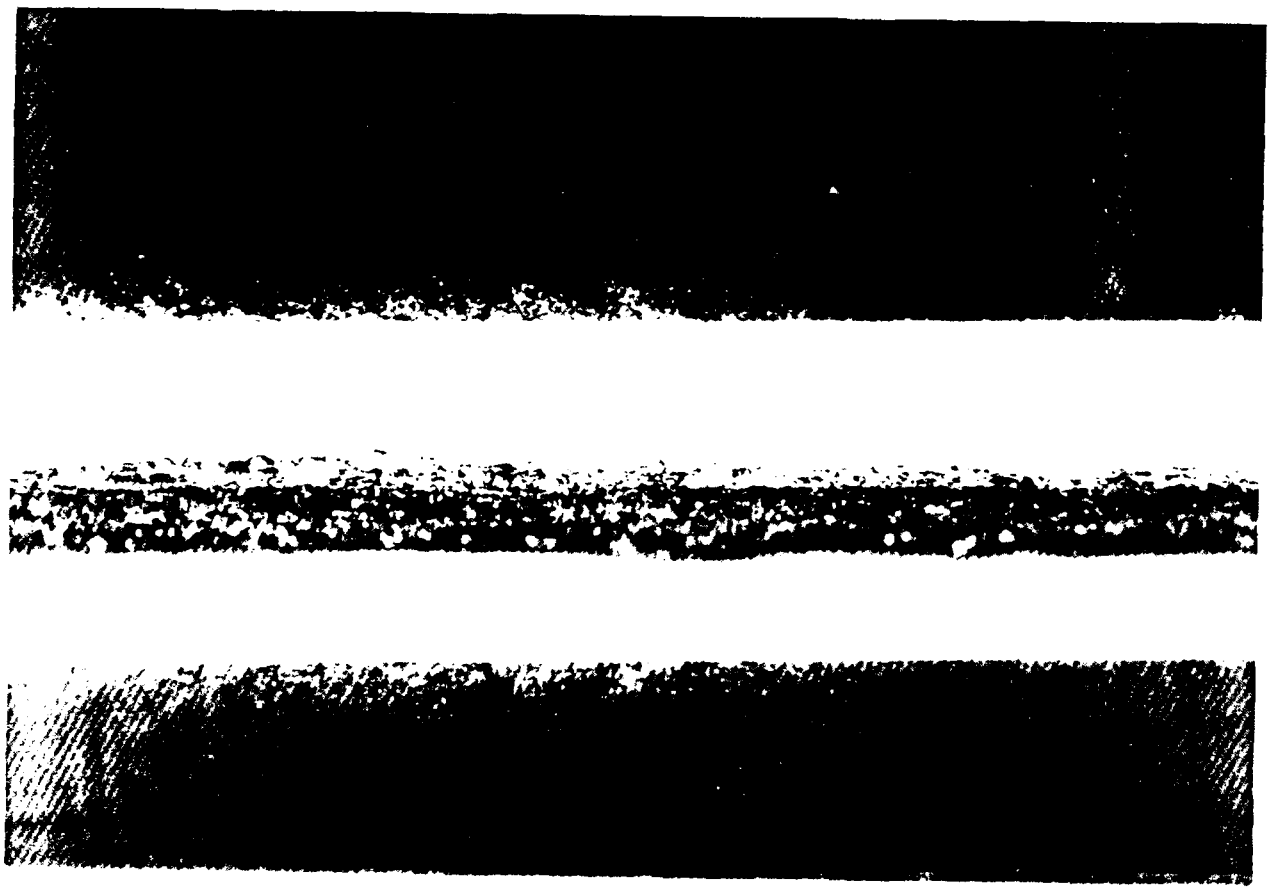

Figure 33 Air jacket ventilation

there once again appears to be some coalescence and separation of the bubbles from the shell surface. Recall from Figure 27, this was the lowest drag condition. Unpublished photographs from ARL/PSU (Merkle & Deutsch, 1989) indicate that, on an axisymmetric body, the bubbles lift away from the body at speeds below 25 ft/s, leading to drag increases.

Figure 33 shows the ventilation occurring due to the large trip used. This effect was not noticed until the tests were well underway and a significant amount of the baseline information had been accumulated. It should be noted from Figures 31 and 32 that ventilation also occurred at the air jacket, with the area affected increasing with speed. A more refined analysis of the drag data will be conducted and presented in later publications (see Coughran et al. [1989]), accounting for the change in wetted area based on underwater photographs.

CONCLUSIONS AND RECOMMENDATIONS

RIBLET EXPERIMENTS

Application of riblets to the shell results in drag reduction from the bare hull condition of up to 3 to 4 percent at the highest velocities (above 12 ft/sec). This is slightly below a first-order prediction based on the NASA data of Walsh and Lindemann [1984] and an assumed transition point at the leading edge of the tape (3 ft aft of the forward perpendicular). Drag reduction is obtained for the lower velocities (less than 12 ft/sec) as well, but only in conditions of high residual turbulence in the tank where low velocity runs immediately followed high velocity runs. In some cases, drag increases are actually obtained. This indicates that for these low velocities, natural transition likely occurs on the riblet surface and is moved forward by residual tank turbulence.

The application of a trip wire to the bare hull produces a parasite drag for low velocities that is well predicted by trip wire drag data found in the literature. On the contrary, an apparent drag reduction of up to 3 percent is produced at the highest velocities. This latter result is unexpected and is speculated to be due to one of

the following mechanisms: changes in sinkage and trim as the hull speed is exceeded, changes in the spray pattern at the bow leading to a possible "spray-lift", or a reduction in wetted surface due to trip wire ventilation.

The maximum drag reduction of greater than 5 percent is achieved through the addition of both riblets and trip wire to the bare hull configuration at the maximum velocity and the middle trip position. This value was slightly lower than the sum of the individual drag reductions of adding the riblets and trip wire, individually. This apparent drag reduction is, however, suspect as described above for the bare hull case.

In any case, riblets appear to be a viable method to reduce viscous drag for surface craft as well as fully submerged marine vehicles and have the potential to yield significant performance enhancement and fuel savings over the long term. In the case of the submarine or torpedo, the application is particularly attractive due to the large friction drag component (approximately 80 percent).

MICROBUBBLE EXPERIMENTS

Due to the compromises made in order to perform the experiment, comparisons with previous laboratory results on simple geometries are difficult. Several physical

differences exist between the present tests and the previous laboratory experiments. These include the presence of a fairly large bubble or blister from which the air was emitted and the use of a surface model with unknown effects on form and wave drag from blowing air into the boundary layer. It is therefore recommended that future experiments employ air injection only from flush-mounted areas in the hull.

Based on the ARL/PSU data, higher test speeds would be desirable for further testing of microbubbles generated by blowing air through porous media. However, a surface model may not operate well at high speeds where the microbubbles presumably become most effective. It may also be possible to support tests of a surface model with analytical/ computational efforts to predict how the form and wave drag are affected by air blowing.

These results present several potential difficulties with the application of this technology to surface craft. It is planned to investigate these questions in future tests, perhaps on an FFG 7 hull, at both USNA and DTRC. The results do not, however, discount the potential benefits for submarine or torpedo applications. In these cases, the axisymmetric data of Deutsch and Castano [Figure 4] may yield a better indication of potential performance.

The electrolysis method of generating bubbles has not

been studied at high speeds. It does, however, require no open pores on the hull and is not as restricted by hydrostatic pressure or air supply, both of which would be major considerations in the submarine and torpedo applications.

ACKNOWLEDGEMENTS

I would like to thank Professor David Coder for his patience and his willingness to put in the long hours. To Professor Roger Compton go my many thanks for always being there to answer the questions and for his guidance and criticism (please, no more red ink!!). To Dr. Mark Coughran, I extend my heartfelt gratitude for his dedication, perserverance, and the sacrifice of many weekends.

I would like to send a special note of thanks to the Hydrolab staff: to John Hill for his guidance and support, to Steve and Don for their help with the pictures and running the carriage, to John Z. and Nancy for their patience with me on the various computers, to Ronnie for bearing the constant interruptions and requests, and to all for being so friendly and supportive.

Finally, I greatly appreciate the understanding and support of family and friends through it all.

REFERENCES

Beauchamp, C.H. and Phillips, R.B.; "Riblet and Polymer Drag Reduction on an Axisymmetric Body", Proceedings of the Symposium on Hydrodynamic Enhancement for Marine Applications, Newport, Rhode Island, October 31-November 1, 1988.

Berman, N.S.; "Laminar Flow in Channels with Porous Walls", Journal of Applied Physics Vol. 24, No. 9, September, 1953, pp.1232-1235.

Bogedevich, V.G. and Malyuga, A.G.; "The distribution of Skin Friction in a Turbulent Boundary Layer in Water Beyond the Location of Gas Injection", in Investigations of Boundary Layer Control (in Russian), edited by S.S. Kutateladze and G.S. Migirenko (Thermophysics Institute Publishing House, Novosibirsk, 1976), p. 62.

Bradel, J.A.; "Air Jacket Structural Analysis Report", DTRC Design Engineering Branch Informal Report, October 21, 1988.

Coder, D.W., et al.; "Drag Reduction with Riblets on Rowing Shells", Accepted for presentation at the 22nd Annual American Towing Tank Conference, St. John's, Newfoundland, August, 1989.

Comstock, J.P.,ed.; Principles of Naval Architecture, New York, The Society of Naval Architects & Marine Engineers, 1967.

Coughran, M.T., et al.; "Application of Microbubbles to a Slender Surface Model", DTRC Report SPD (in preparation).

Deutsch, S. and Castano, J.; "Microbubble Skin Friction Reduction on an Axisymmetric Body", Physics of Fluids, Vol. 29, November, 1986, pp. 3590-3597.

Dubnishev, Yu., et al.; "Study of Gas-Saturated Turbulent Streams Using a Laser-Doppler Velocimeter", Journal of Applied Mechanics and Technical Physics 16, No. 1, 1975, p. 114. Translated from Zhur. Prikl. Mech. Tekh. Phys., No. 1, 1975, p. 147.

Eilers, R.E., et al.; "An Application of Riblets for Turbulent Skin Friction", 12th Annual Symposium on Sailing, AIAA, University of Washington, Seattle, WA, September, 1985.

Gillmer, T.C. and Johnson, B.; Introduction to Naval Architecture, Annapolis: Naval Institute Press, 1982.

Granville, P.; "The Determination of the Local Skin Friction and the Thickness of Turbulent Boundary Layers", David Taylor Model Basin Report 1340, 1959.

Hartnett, J.P., et al.; "A Comparison of Predicted and Measured Friction Factors for Turbulent Flow Through rectangular ducts", Transactions of the ASME, February, 1962, pp. 82-88.

International Towing Tank Conference Catelogue of Facilities, Proceedings of the 16th ATTC, 1971, the 18th ATTC, 1977, and the 19th ATTC, 1980.

Koslov, L.F.; "Investigation of the Boundary Layer Turbulence Stimulation of Ship Models", 12th Annual International Towing Tank Conference, Rome, Italy, 1969.

Madavan, N.K.; "The effects of microbubbles on turbulent boundary layer skin friction", Ph.D. Thesis, Dept. of Mechanical Engineering, The Pennsylvania State University, 1984.

Madavan, N.K., Deutsch, S., and Merkle, C.L.; "The effects of porous material on microbubble skin friction reduction", TM 83-202, Applied Research Laboratory, Pennsylvania State University. Also AIAA Paper 84-0348, presented at 22nd AIAA Aerospace Sciences Mtg, Reno, Nevada, 1984.

Madavan, N.K., et al.; "Measurements of local skin friction in a microbubble-modified turbulent boundary layer", Journal of Fluid Mechanics (1985), Vol. 156, pp.237-256.

MMC Brochure; Precision Porous Metals Engineering Guide, DB1000, Mott Metallurgical Corporation, Farmington Industrial Park, Farmington, Connecticut 06032, 1988.

McCarthy, J.H., Power, J.L., and Huang, T.T.; "The Roles of Transition, Laminar Separation, and Turbulence Stimulation in the Analysis of Axisymmetric Body Drag", Eleventh Annual Symposium on Naval Hydrodynamics, London, England, 1976.

McCormick, M.E. and Bhattacharya, R.; "Drag Reduction of a Submersible Hull by Electrolysis", Naval Engineers Journal 85, 1973, pp. 11-16.

McCormick, M.E.; Personal communication, Department of Naval Systems Engineering, United States Naval Academy, Annapolis, Maryland 21402, 1989.

McKelvey, D.; "An Experimental Analysis of Riblet Application for Turbulent Drag Reduction", USNA Division of Engineering and Weapons Report, 1988.

Merkle, C.L.; "Microbubble Drag Reduction", 16th Annual Symposium on Naval Hydrodynamics, 1986.

Merkle, C.L. & Deutsch, S.; Personal communication, Applied Research Laboratory, The Pennsylvania State University, College Park, Pennsylvania, 1989.

Migirenko, G.S., et al.; "Turbulent Boundary Layer with Gas Saturation", Problems of Thermophysics and Physical Hydrodynamics (in Russian), (Novosibirsk), Nauka, 1974.

Reidy, L.W. and Anderson, G.W.; "Drag Reduction for External and Internal Boundary Layers Using Riblets and Polymers", AIAA-88-0138, 26th Aerospace Sciences Meeting, Reno, NV, January 1988.

Thornton, W.A.; "Drag reduction of a hull by electrolysis", U.S. Naval Academy Trident Scholar Project Report No. 63, 1974.

Walsh, M.J. and Lindemann, A.M.; "Optimization and Application of Riblets for Turbulent Drag Reduction", AIAA-84-0347, AIAA 22nd Aerospace Sciences Meeting, Reno, NV, January 9-12, 1984.

White, F.M., Barfield, B.F. & Goglia, M.J.; "Laminar flow in a uniformly porous channel", Trans. ASME Journal of Applied Mechanics, 613, 1958.

Yuan, S.W.; "Turbulent flow in channels with porous walls", Journal of Mathematics and Physics **38**, 166, 1959.

APPENDIX:

ROWING SHELL CHARACTERISTICS

Table A.1.: White shell data

Length:
wl 25' 7.5"
oa 26' 6.4"

Wetted Surface Area:

Station	Girth port	Girth stbd	Girth total	Entire Shell Girth odd	Entire Shell Girth even
ft	in	in	in		
.00	.00	.00	.13		
.63	1.25	1.25	2.63		
1.63	2.13	2.19	4.45	4.45	
2.63	3.06	3.07	6.26		6.26
3.63	3.97	3.99	8.09	8.09	
4.63	4.81	4.87	9.81		9.81
5.63	5.69	5.73	11.55	11.55	
6.63	6.38	6.44	12.95		12.95
7.63	7.03	6.99	14.15	14.15	
8.63	7.53	7.50	15.16		15.16
9.63	8.06	7.94	16.13	16.13	
10.63	8.38	8.30	16.81		16.81
11.63	8.56	8.38	17.07	17.07	
12.63	8.68	8.55	17.36		17.36
13.63	8.81	8.63	17.57	17.57	
14.63	8.81	8.69	17.63		17.63
15.63	8.62	8.56	17.31	17.31	
16.63	8.27	8.41	16.81		16.81
17.63	7.93	8.09	16.15	16.15	
18.63	7.53	7.66	15.32		15.32
19.63	7.13	7.24	14.50	14.50	
20.63	6.61	6.63	13.37		13.37
21.63	5.86	5.94	11.93	11.93	
22.63	4.98	5.03	10.14		10.14
23.63	3.89	3.83	7.85	7.85	
24.63	2.77	2.63	5.53		
25.63	1.47	1.31	2.91		

Simpson's Rule Approximations

s0	s1	s2
8.15	156.69	151.57

Station	WSA sq. in.		
0-0.46	10.31		
0.46-24.46	3752.16		
24.46-25.46	50.58		
Total	3813.05	=	26.48 sq. ft.

Table A.1: White shell data

Center of floation/tpi/mtl":

Station	beam	Flotation Area aft of station 0	Moment of Inertia
ft	in	sq in	ft^4
.00	.13	.00	.48
.63	1.42	5.79	9.97
1.63	3.72	36.63	35.33
2.63	5.58	92.43	43.53
3.63	7.22	169.23	45.28
4.63	8.76	265.11	43.00
5.63	9.78	376.35	36.31
6.63	10.48	497.91	28.13
7.63	10.94	626.43	19.93
8.63	11.48	760.95	12.92
9.63	11.66	899.79	6.95
10.63	11.96	1041.51	2.80
11.63	12.10	1185.87	.46
12.63	12.00	1330.47	.11
13.63	11.68	1472.55	1.71
14.63	11.48	1611.51	5.17
15.63	11.30	1748.19	10.41
16.63	10.88	1881.27	16.96
17.63	10.18	2007.63	24.06
18.63	9.42	2125.23	31.40
19.63	8.60	2233.35	38.45
20.63	7.40	2329.35	42.74
21.63	6.16	2410.71	44.64
22.63	4.86	2476.83	43.18
23.63	3.34	2526.03	35.70
24.63	1.78	2556.75	22.53
25.63	.13	2568.18	.88

Center of Floation:
12.30ft aft of station 0

Tonnes per in (lbf/in):
92.74 lbf/in

Moment of Inertia:
603.01 ft^4

Moment to trim 1":
125.96 ft-lbf

Table A.2.: Yellow shell data

Length:
wl 25' 5.5"
oa 26' 6.5"

Wetted Surface Area:

			Entire shell			Forward of Air Jacket	
Station	Girth port	Girth stbd	Girth total	Girth odd	Girth even	Girth odd	Girth even
ft	in	in	in				
.00	.00	.00	.13				
.46	.92	.98	2.03				
1.46	2.42	2.40	4.95	4.95		4.95	
2.46	3.84	3.58	7.55		7.55		7.55
3.46	5.06	4.72	9.91	9.91		9.91	
4.46	5.84	5.62	11.59		11.59		11.59
5.46	6.56	6.38	13.07	13.07		13.07	
6.46	7.20	6.92	14.25		14.25		14.25
7.46	7.66	7.46	15.25	15.25		15.25	
8.46	8.16	7.94	16.23		16.23		16.23
9.46	8.46	8.26	16.85	16.85		16.85	
10.46	8.72	8.46	17.31		17.31		17.31
11.46	8.92	8.60	17.65	17.65		17.65	
12.46	8.88	8.60	17.61		17.61		17.61
13.46	8.88	8.50	17.51	17.51		17.51	
14.46	8.74	8.38	17.25		17.25		
15.46	8.46	8.14	16.73	16.73			
16.46	8.06	7.86	16.05		16.05		
17.46	7.52	7.42	15.07	15.07			
18.46	7.06	6.90	14.09		14.09		
19.46	6.32	6.34	12.79	12.79			
20.46	5.70	5.64	11.47		11.47		
21.46	4.92	4.88	9.93	9.93			
22.46	3.98	4.00	8.11		8.11		
23.46	3.06	3.02	6.21	6.21			
24.46	2.04	2.08	4.25				
25.46	1.08	1.18	2.39				

Simpson's Rule Approximations

Entire shell			Forward of Air Jacket		
s0	s1	s2	s0	s1	s2
6.27	155.86	151.46	19.27	95.16	84.51

Station	WSA sq. in.	Station	WSA sq. in.
0-0.46	5.91	0-.46	5.91
0.46-24.46	3730.48	0.46-14.46	2275.64
24.46-25.46	39.78		
Total	3776.17	Total	2281.55
WSA =	26.22 sq. ft.	WSA =	15.84 sq. ft.

Percentage of WSA aft of air jacket: 39.58 %

Table A.2.: Yellow shell data

Center of floation/tpi/mtl":

Station	beam	Flotation Area aft of station 0	Moment of Inertia
ft	in	sq in	ft^4
.00	.13		.36
.46	.75	2.40	6.02
1.46	3.25	26.40	32.07
2.46	5.38	60.15	43.74
3.46	7.22	117.72	47.47
4.46	8.54	212.28	44.21
5.46	9.50	320.52	37.49
6.46	10.32	439.44	29.75
7.46	10.88	566.64	21.61
8.46	11.40	700.32	14.32
9.46	11.68	838.80	8.08
10.46	11.94	980.52	3.52
11.46	11.98	1124.04	.78
12.46	11.94	1267.56	.01
13.46	11.68	1409.28	1.22
14.46	11.48	1548.24	4.29
15.46	11.28	1684.80	9.14
16.46	10.80	1817.28	15.26
17.46	10.10	1942.68	22.05
18.46	9.36	2059.44	29.20
19.46	8.62	2167.32	36.40
20.46	7.36	2263.20	40.42
21.46	6.20	2344.56	42.95
22.46	4.76	2410.32	40.61
23.46	3.30	2458.68	33.99
24.46	1.80	2489.28	22.03
25.46	.13	2500.83	.86

Center of Floation:
12.34ft aft of station 0

Tonnes per in (lbf/in):
90.31 lbf/in

Moment of Inertia:
587.85 ft^4

Moment to trim 1":
123.15 ft-lbf

Figure A.1. Rowing shell shear view

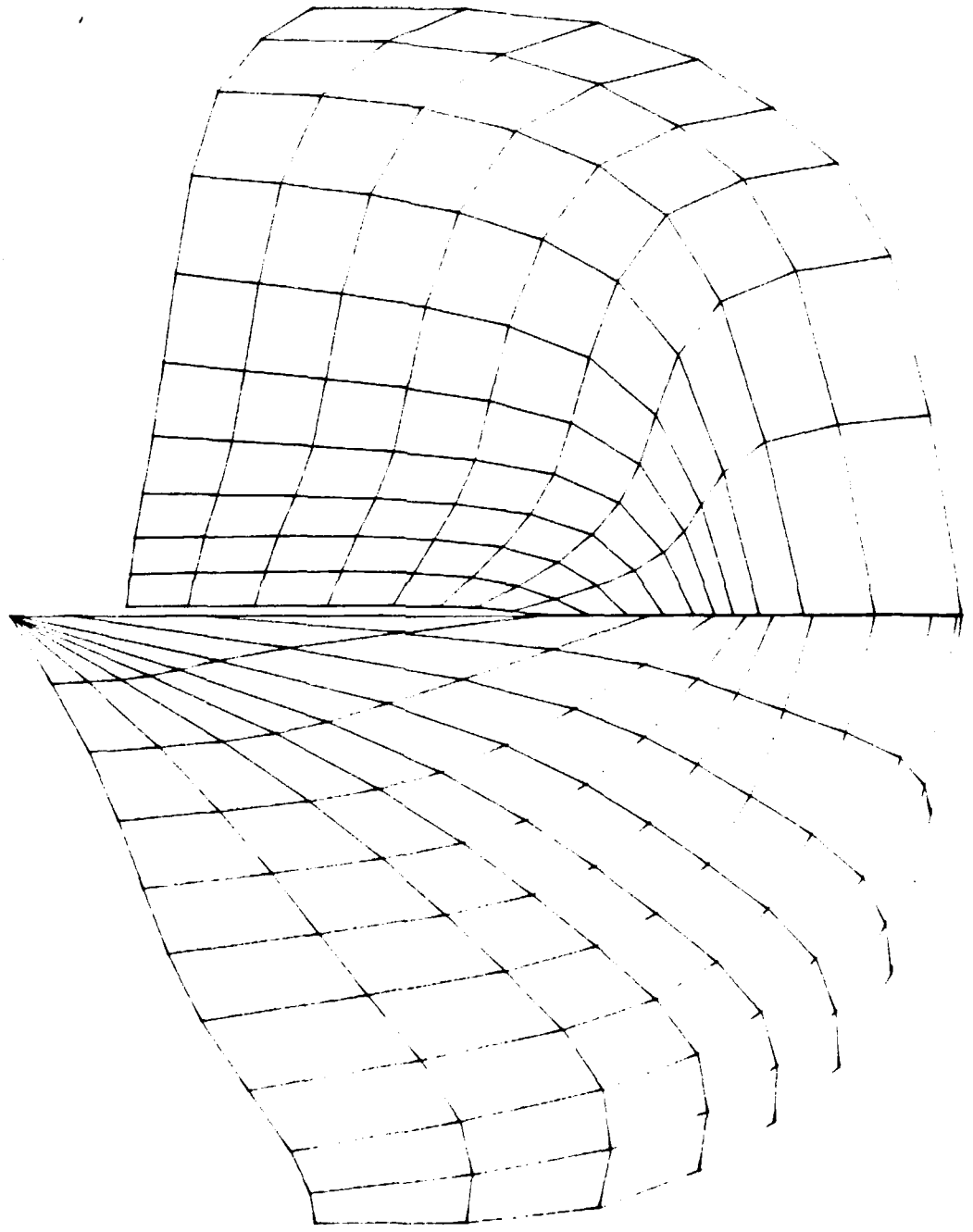

Figure A2. Rowing shell body plan

Figure A.3. Rowing shell planview

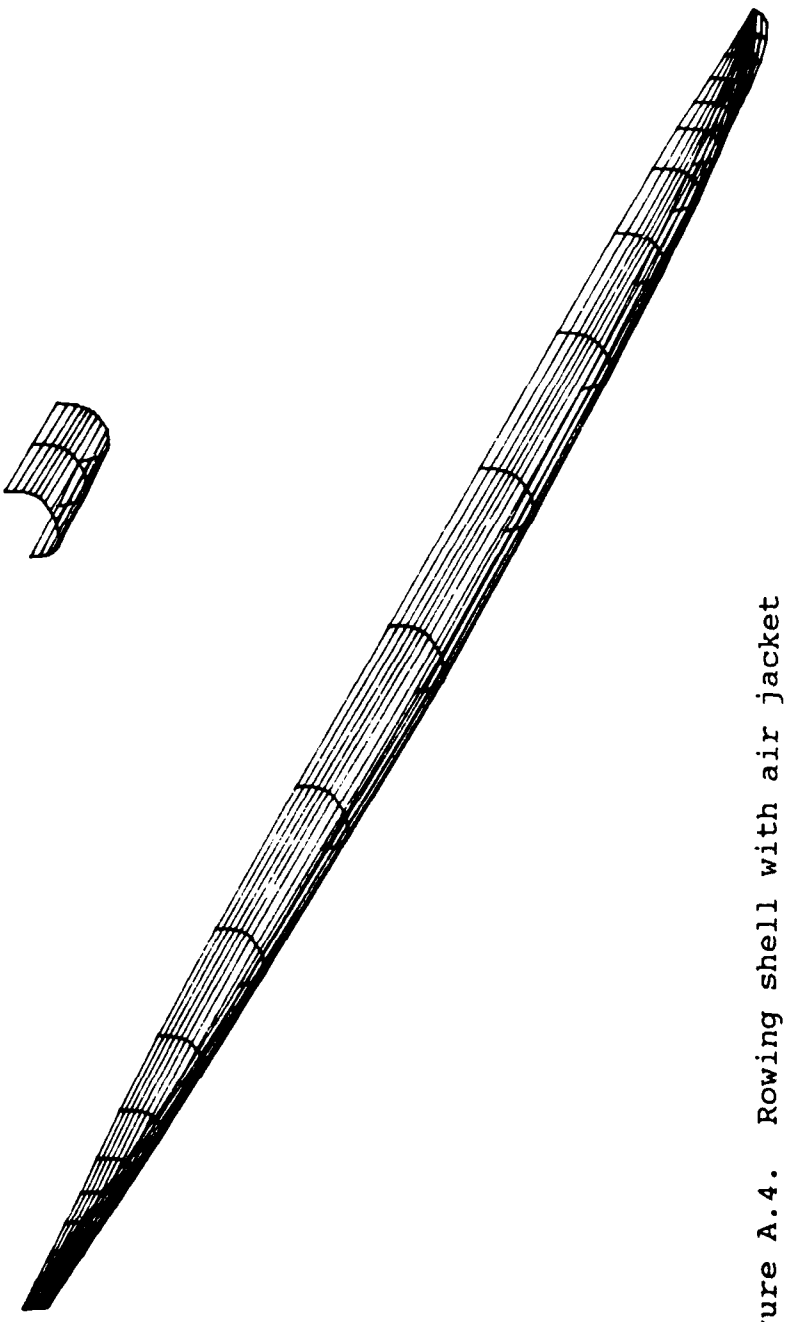

Figure A.4. Rowing shell with air jacket

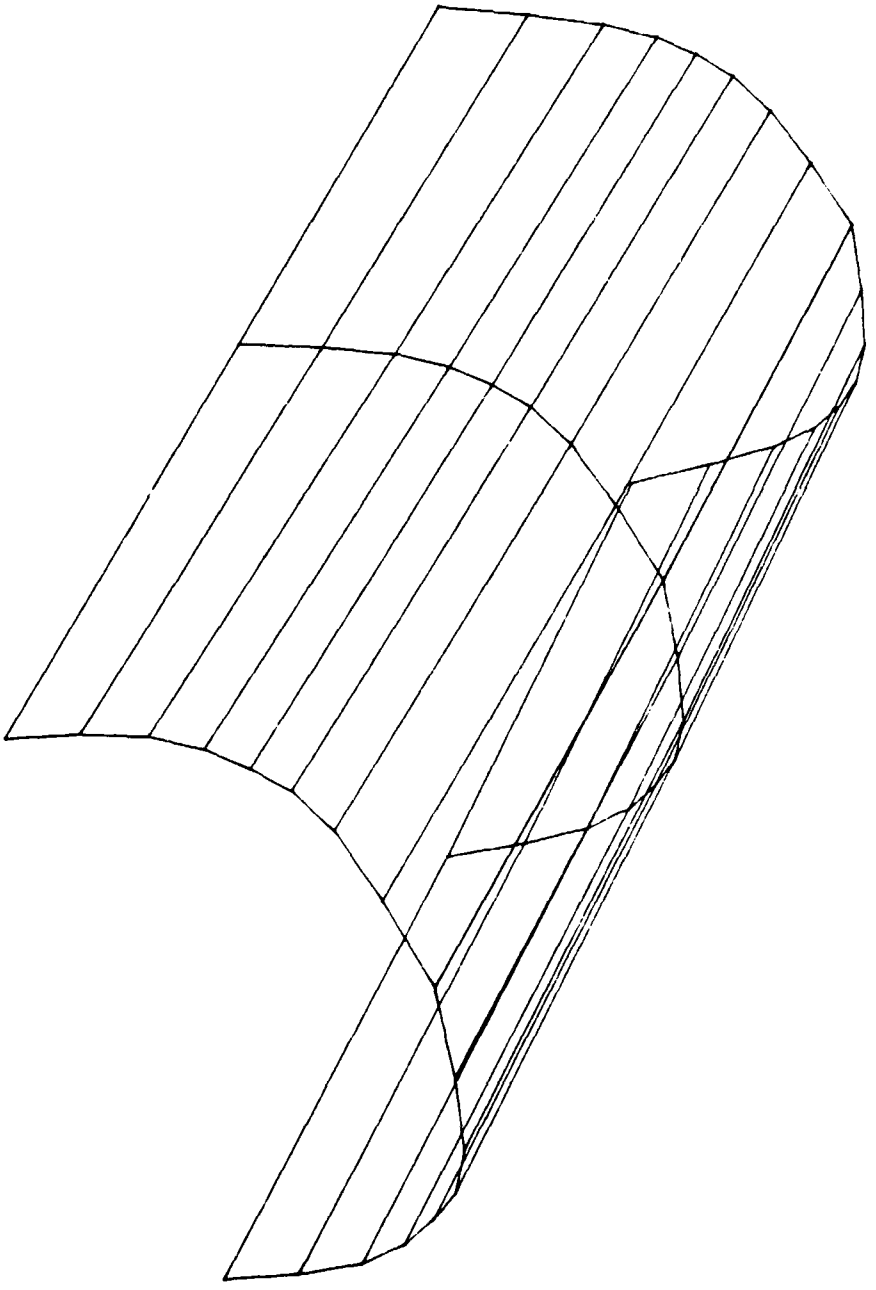

Figure A.5. Air jacket